ACS ORGANIC & INORGANIC Au
AN OPEN ACCESS JOURNAL OF THE AMERICAN CHEMICAL SOCIETY

pubs.acs.org/orginorgau

Article

Triazolyl- vs Pyridyl-Functionalized *N*-Heterocyclic Carbene Complexes: Impact of the Pendant N-Donor Ligand on Intramolecular C−C Bond Formation

Betty Y.T. Lee, Andrew D. Phillips,* Muhammad Hanif, Tilo Söhnel, and Christian G. Hartinger*

Cite This: *ACS Org. Inorg. Au* 2022, 2, 511−524

Read Online

ACCESS | Metrics & More | Article Recommendations | Supporting Information

ABSTRACT: Organometallic Rh(Cp*) (Cp* = η^5-pentamethylcyclopentadienyl) complexes with monodentate *N*-heterocyclic carbene (NHC) ligands bearing a pendant anthracenyl substituent have been shown to undergo intramolecular C−C coupling reactions. Herein, two bidentate NHC ligands substituted with pyridyl or triazolyl donor groups were prepared along with the corresponding $M^{II/III}$ (M = Ru^{II}, Os^{II}, Rh^{III}, Ir^{III}) complexes. While the Rh(Cp*) complex featuring an NHC-triazole bidentate ligand underwent the equivalent reaction as the monodentate Rh(NHC) complex, *i.e.*, it formed a polydentate ligand, the pyridyl-pendant derivative was unequivocally shown to be unreactive. This contrasting behavior was further investigated by density functional theory (DFT) calculations that highlighted significant differences between the two types of Rh(III) complexes with pendant pyridyl or triazolyl *N*-coordinating groups. Modeling of the reaction pathways suggests that the initial formation of a dicationic Rh(III) species is unfavorable and that the internal ligand transformation proceeds first by dissociation of the coordinated N atom of the pendant group from the Rh center. After the formation of a neutral η^4-fulvene ligand *via* combined proton/single electron transfer, a cycloaddition occurs between the exo-ene bond of fulvene and the 9′ and 10′ positions on the pendant anthracenyl group. The resulting experimental UV−visible spectrum recorded in methanol of the polydentate triazolyl-based Rh species revealed the loss of the vibronic coupling typically associated with an anthracenyl functional group. Moreover, TD-DFT modeling indicates the presence of an equilibrium process whereby the *N*-coordination of the pendant triazolyl group to the Rh^{III} center appears to be highly labile. Charge decomposition analysis (CDA) of the DFT-modeled species with the dissociated triazolyl group revealed a pseudo-η^3-allylic interaction between the π-type MOs of the transformed anthracenyl group and the Rh^{III} center; thus, the singly attached chelating ligand is classified as having rare nonadenticity.

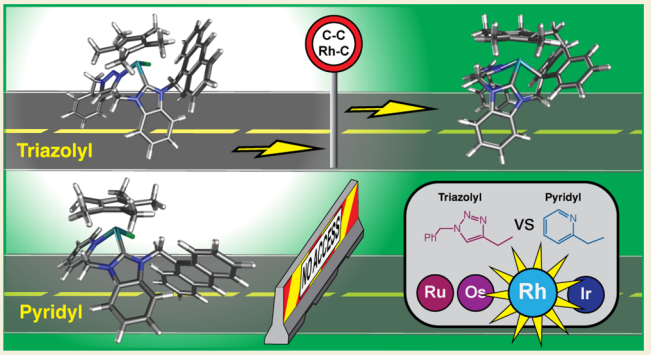

KEYWORDS: *NHC complexes, pendant ligand, intramolecular reaction, bio-organometallic chemistry, reaction mechanism*

INTRODUCTION

N-Heterocyclic carbene (NHC) complexes have recently been investigated as anticancer agents.[1,2] Compounds based on Au,[3] Ag,[4] Cu,[5] Ir,[6] Rh,[7] Os,[1] and Ru[8,9] have been studied and shown to exhibit anticancer activity *via* mechanisms different to that of cisplatin which is widely used in clinics.[10] We and others have reported half-sandwich organometallic compounds featuring NHC ligands that inhibit thioredoxin reductase.[11−15] Ru^{II}(η^6-arene) compounds such as the RAPTA and RAED families belong to the class of half-sandwich compounds and have demonstrated potential as anticancer chemotherapeutics,[16,17] as have many other analogs.[18−21] RAPTA-C containing a 1,3,5-triaza-7-phosphaadamantane (pta) ligand is a metastasis inhibitor that forms adducts on histone proteins,[22] while RAED-C with its bidentate ethylenediamine ligand targets DNA of chromatin.[22] The potential of these Ru complexes led to the development of isostructural Os(II),[23,24] Rh(III),[25] and Ir(III)[26] derivatives that exhibit different ligand exchange kinetics and preferences for donor atoms on biological targets.

Other metals from the platinum metal family, in particular, Ir, Os, Rh, and Ru, are employed in the design of novel metal−NHC compounds. We have recently reported a series of [M(L)(NHC)Cl_2] complexes (where M = Ru, Os, Rh, Ir; L = η^6-*p*-cymene [cym], η^5-pentamethylcyclopentadienyl [Cp*]) with an *N*-flanking anthracenyl moiety attached to the NHC ligands, and the complexes showed excellent cytotoxic activity.[27] We have shown that the anthracenyl-functionalized

Received: July 7, 2022
Revised: August 29, 2022
Accepted: August 29, 2022
Published: September 20, 2022

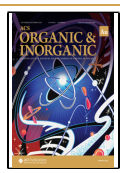

https://doi.org/10.1021/acsorginorgau.2c00035
ACS Org. Inorg. Au 2022, 2, 511−524

NHC−Ru^{II}(cym) complex forms adducts with hen egg white lysozyme by binding to an Asp residue and a π-stacking interaction with a Trp residue.[27] Interestingly, we showed that [Rh(Cp*)(NHC-anthracenyl)Cl_2] **A** can undergo intramolecular C−C coupling, forming complex **B** (Figure 1) with a

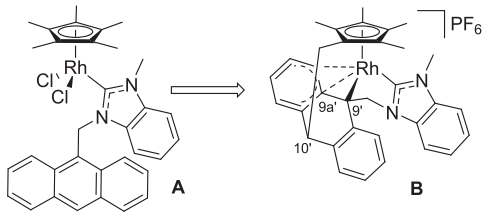

Figure 1. Chemical structure of **B**, formed in an intramolecular C−C coupling reaction involving [Rh(Cp*)(NHC-anthracenyl)Cl_2] **A**.[27,28]

seemingly nonadentate all-carbon donor atom ligand.[27,28] This involves the activation of the Cp* ligand for reactions at the methyl groups,[29−31] which also led to intramolecular cross-coupling reactions in Rh(Cp*)(NHC) complexes with an *N*-methylpyridinium-[29] and pentafluorobenzyl-functionalized NHC ligand.[31] To alter the properties of such compounds, we introduce here pyridyl or triazolyl functional groups to the anthracenyl-NHC ligand system, converting them into bidentate ligand systems with coordination *via* a *C,N*-donor system. We have investigated these species in terms of their reactivities and structural features, in particular with respect to undergoing intramolecular reactions in analogy to **A**.

RESULTS AND DISCUSSION

Intrigued by the intramolecular C−C coupling reaction observed for [Rh(Cp*)(NHC-anthracenyl)Cl_2] **A** that led to **B**,[27,28] we aimed to explore bidentate anthracenyl-substituted pro-carbenes featuring in addition a pyridyl or triazolyl functional group as ligands for half-sandwich organometallics (Scheme 1). The preparation proceeded from the precursors 1-(pyridin-2-ylmethyl)benzimidazole **1** or (9-anthracenylmethyl)benzimidazole **2** by *N*-alkylation with 9-chloromethylanthracene or propargyl bromide to yield **4** and **3**, respectively. The latter was converted into the triazolyl-functionalized pro-carbene **5**, through a copper(I)-catalyzed azide alkyne cycloaddition (CuAAC) with benzyl azide in the presence of copper(II) sulfate and L-ascorbate.[32] Compounds **1**−**5** were obtained in high yields, and the structures were confirmed by ^{1}H NMR spectroscopy, as well as $^{13}C\{^1H\}$ NMR and 2D NMR spectroscopy for both pro-carbenes **4** and **5**.

Scheme 1. Synthetic Pathways to Precursors and (Anthracenyl-NHC)$M^{II/III}$(cym/Cp*) Complexes

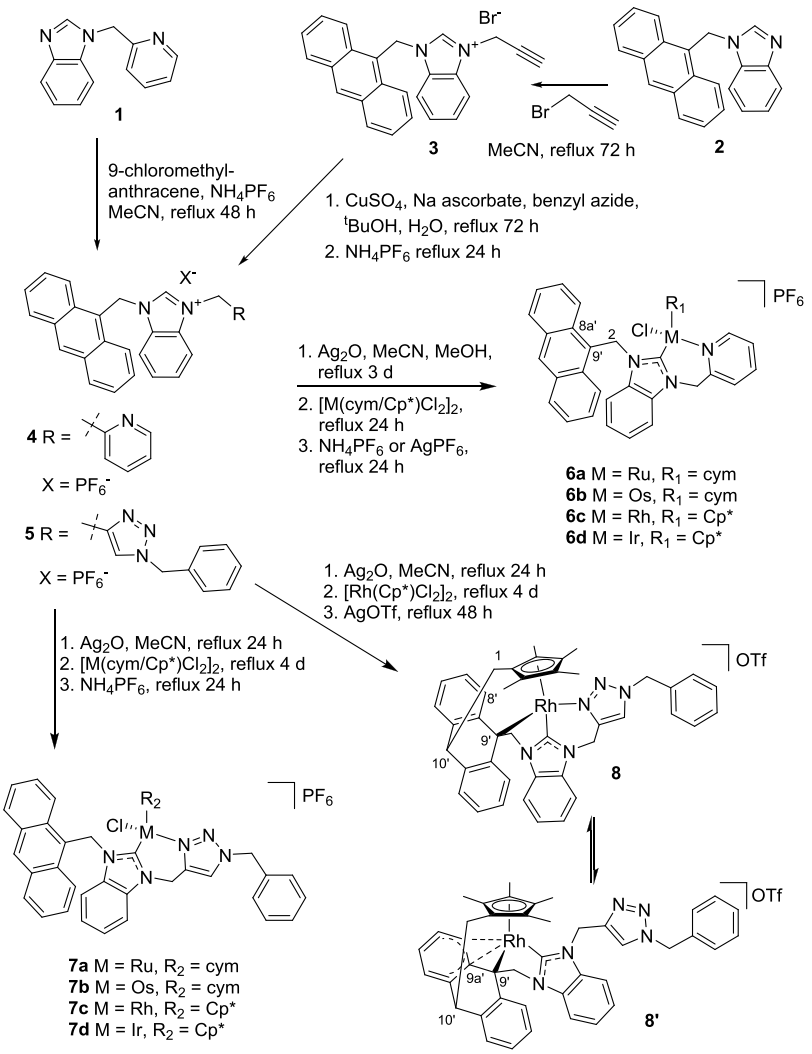

https://doi.org/10.1021/acsorginorgau.2c00035
ACS Org. Inorg. Au 2022, 2, 511−524

Precursors **3**−**5** were further characterized by electrospray ionization mass spectrometry (ESI-MS; Table S1). The experimental *m/z* values were in good agreement with the theoretical values. The most abundant peaks observed in the ESI-mass spectra were assigned to $[M - Br]^+$ or $[M - PF_6]^+$ ions.

The pro-carbenes **4** and **5** were coordinated to $M^{II/III}$(cym/Cp*)Cl moieties (M = Ru^{II}, Os^{II}, Rh^{III}, Ir^{III}) using silver-mediated transmetalation.[1] Compounds **4** and **5** were activated using Ag_2O followed by addition of $[M^{II/III}(cym/Cp^*)Cl_2]_2$ and treatment with $AgPF_6$ or NH_4PF_6 for counterion exchange, which yielded the orange or yellow complexes **6a**−**d** and **7a**−**d** in 24−54% with the ligands coordinated bidentately to the metal center (Scheme 1). An attempt to prepare **7c** from **5** but with OTf^- instead of PF_6^- as the counterion resulted in the formation of a blue product after workup, similar to the observations found in the conversion of $[Rh(Cp^*)(NHC\text{-anthracenyl})Cl_2]$ **A** to **B**.[27,28] The signals of the Cp* protons in the ^{1}H NMR spectrum, which were expected to be found as a singlet at ca. 1.8 ppm for **7c**, could not be assigned to the expected structure. In contrast, the Cp* protons were detected as three signals at 0.40, 1.77, and 2.22 ppm, suggesting the formation of Rh complex **8** or, in analogy to **B**,[28] of **8′** (Scheme 1; 38% yield). We hypothesize that the activation of a Cp* methyl group of Rh(Cp*) complexes led to an intramolecular C−C coupling with the anthracenyl moiety of the NHC ligand, as observed for **B** (Figure 1),[27,28] subsequently resulting in a polydentate ligand coordinated to the Rh center (Scheme 1). In analogy to **B**, we suggest that the Rh complex contains a pseudo-nonadentate ligand formed from the carbon donor atoms of the benzimidazol-2-ylidene, anthracenyl, and Cp* moieties (Scheme 1). Indeed, the comparison of the ^{1}H NMR spectrum with that of **B** shows a high level of similarity for the relevant parts, in particular with what we would expect for the triazolyl moiety not coordinated as in **8′** (Scheme 1, Figure 2). The transformed Cp* signals were comparable, suggesting that the compound also underwent a C1−C10′ coupling reaction after deprotonation of one of the Cp* methyl groups, and the ^{1}H NMR spectrum lacked the geminal coupling observed for the protons of the CH_2 group bridging the NHC and triazole, suggesting a higher structural flexibility in the polydentate ligand. Therefore, we suggest that **8′** was formed, possibly after the initial formation of **8**. Density functional theory calculations show an energy difference of just 1.35 kcal mol^{-1} between **8** and **8′** (*vide infra*), and therefore, this seems to be a feasible pathway, although the two species may be present in equilibrium.

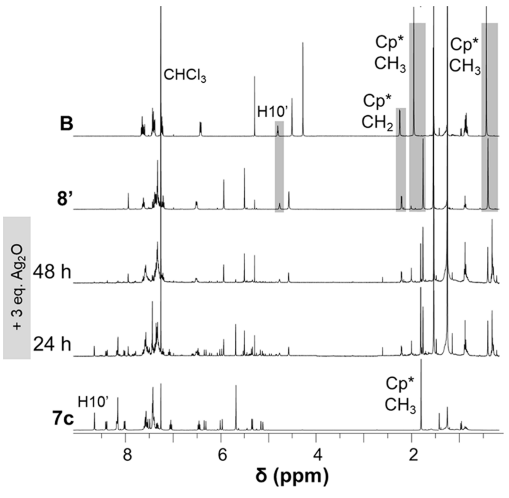

Figure 2. ^{1}H NMR spectroscopic study on the reaction of **7c** with 3 equiv Ag_2O over a period of 48 h and, for comparison, the spectra of **7c**, **8′**, and **B** in $CDCl_3$.

Compound **7c** could be converted to **8′** by reaction with Ag_2O in DCM under reflux for 24 h (Figure 2 and Figure S1, Table S2), while the treatment with AgOTf did not result in the formation of **8′**, as indicated by ^{1}H NMR spectroscopy and the highly characteristic color change of the solution to blue. These observations are consistent with the suggested mechanism for the formation of **B** involving a $Rh^I(\eta^4$-fulvene) intermediate with the Ag_2O acting as the base to deprotonate the Cp* ligand.[28] Moreover, a Rh−C9′ bond was expected to form after abstraction of the chlorido ligand by Ag^+ for complex **8′** as was demonstrated for **B** crystallographically. The same set of experiments was conducted for the other triazolyl complexes (**7a**, **7b**, **7d**) as well as the pyridyl derivatives **6a**−**6d**, but neither color changes to blue nor any changes in the ^{1}H NMR spectra were observed, indicating the importance of the Rh center in the reaction. The complexes were also characterized by 2D NMR spectroscopy, ESI-mass spectrometry, and elemental analysis. In the $^{13}C\{^1H\}$ NMR spectra, some quaternary and aromatic carbon atoms could not be detected even with high numbers of scans and were assigned based on HSQC and HMBC analysis. Some of the elemental analyses indicated the presence of solvents, which were also detected by NMR spectroscopy. The ESI-mass spectra of complexes **6a**−**d**, **7a**−**d**, and **8′** featured pseudo-molecular ions assignable to $[M - PF_6]^+$ or $[M - OTf]^+$ ions, and the observed *m/z* values were in good agreement with the calculated ones (Table S1).

X-ray diffraction analysis data of single crystals of pro-carbene **4** and complex **6a** obtained from deuterated chloroform (Figure 3 and Figure S2) showed that **6a**

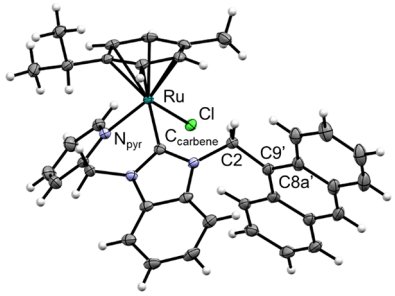

Figure 3. Molecular structure of one of the two crystallographically independent molecules of complex **6a**, drawn at 50% probability level, with the numbering scheme used for the discussion. The PF_6^- counterion and co-crystallized solvent were omitted for clarity.

crystallized in the monoclinic space group $P2_1/n$ and **4** in *Pn*. The latter showed π-stacking between the anthracene and the benzimidazolium moieties, and the pyridyl groups were disordered with ratios of 63(1):37(1) and 55(2):45(2) for the two independent molecules. Complex **6a** was found as two crystallographically independent molecules, each forming two enantiomeric molecules that feature a piano-stool geometry with bond lengths similar to Ru−NHC complexes bearing a pyridyl group.[8,33] The $Ru-C_{carbene}$, $Ru-N_{pyr}$, and Ru−Cl distances of **6a** (Figure 3) of one of the two independent

https://doi.org/10.1021/acsorginorgau.2c00035
ACS Org. Inorg. Au 2022, 2, 511−524

molecules were found at 2.038(2), 2.116(2), and 2.3889(4) Å, respectively (Table 1), and were very similar to the bond lengths reported for the structurally related Ph-substituted compound **6a**^{Ph}.[8] The coordination of the bidentate ligands to the metal center led to the formation of six-membered metallaring systems, while the anthracenyl substituent of the ligand was twisted with a torsion angle (N−C2−C9′−C8a′) of 129.41°. The Ru−arene$_{centroid}$ distance was found at 1.726 Å, and the bond angles Cl−Ru−C$_{carbene}$, Cl−Ru−N$_{pyr}$, and N$_{pyr}$−Ru−C$_{carbene}$ of **6a** were 87.33(5), 84.41(4), and 84.90(7)°, respectively, again very similar to **6a**^{Ph} (Table 1).[8] The benzylidene group of one molecule of **6a** was found to form π-stacking interactions with a coordinated pyridine moiety of another molecule with 3.257 Å as the shortest distance.

Table 1. Key Bond Lengths (Å) and Angles (°) for Complex 6a in Comparison to the Phenyl-Substituted Analog 6a^{Ph}[8]

compound	6a	6a^{Ph}[a]
	bond lengths (Å)	
Ru−C$_{carbene}$	2.038(2)	2.039(6)
	2.045(2)[b]	
Ru−N$_{pyr}$	2.116(2)	2.114(2)
	2.108(2)[b]	
Ru−Cl	2.3899(4)	2.414(1)
	2.3906(4)[b]	
	bond angles (°)	
Cl−Ru−C$_{carbene}$	87.33(5)	87.80
	87.79(5)[b]	
Cl−Ru−N$_{pyr}$	84.41(4)	84.69
	84.04(4)[b]	
N$_{pyr}$−Ru−C$_{carbene}$	84.90(7)	85.31
	85.74(7)[b]	
	torsion angles (°)	
N−C2−C9′−C8a′	129.41	173.25
	−122.11[b]	

[a]Obtained from ref 8. [b]Two independent molecules were found in the crystal structure.

To further investigate the bonding in **8** and **8′**, computational studies were conducted (a) to establish the relative stability of the complexes featuring the combined carbene-triazolyl and -pyridyl ligands with respect to different metal centers (*i.e.*, Ru, Os, Rh, and Ir) and (b) to provide a rationale for the experimentally observed difference in chemical behavior between the Rh carbene-triazole complex **7c** that transforms into **8**/**8′** and the corresponding Rh carbene-pyridyl species **6c** that remains chemically inert and does not undergo fulvene formation or an internal interligand coupling through a metallo-cycloaddition process.

To investigate the reactivity of **8′** further, we incubated it with 1,3,5-triaza-7-phosphaadamantane (pta; Scheme 2) and followed the reaction with ^{1}H and ^{31}P{^{1}H} NMR spectroscopy, ESI-MS, and DFT calculations (Figures S3−S6). The ESI-mass spectrum (Figure S3) supported the formation of the pta derivative **8**^{pta} with the Cp*/NHC/triazolyl-derived ligand as well as pta coordinating to the Rh center. The spectrum showed a peak at *m/z* 873.3024 that was assigned to [**8′** − OTf + pta]$^{+}$ (m$_{calc}$ = 873.3024). The ^{31}P{^{1}H} NMR spectrum (Figure S5) of the reaction mixture of **8′** and pta gave a doublet at −46.6 ppm ($^{1}J_{Rh-P}$ = 150 Hz), which is in good agreement with the chemical shifts previously reported for analogous derivatives[28] and indicates the coordination of pta to Rh. These studies imply that the interactions of Rh with the anthracenyl group other than with C9′ are weak and can be easily broken by addition of a ligand such as pta. This also supports the notion of the triazolyl moiety in **8** being weakly coordinated to Rh and suggests that the metallo-cycloaddition product is actually **8′** rather than **8**, which may also exist in equilibrium due to minor energetic differences (*vide supra*).

To assess relative ligand−metal bond stability, calculation of the Mayer-bond indices is extremely useful as these values are normalized and hence different bond types are directly comparable. The analysis involved geometry optimization of each complex cation to an energy minimum using the ω-B97xD DFT methodology that includes long-range dispersion effects and a basis set where a pseudopotential is employed for each metal (SDDAll). Full details of the optimization procedure are as reported previously with details on the benchmarking process given in the Supporting Information (Figures S7−S9, Tables S3 and S4).[28] Figure 4 provides a comparison of the collective bond orders around each metal to Cp*, Cl, C(carbene), and N(triazolyl or pyridyl), with the sum of the bond order indicating the total bond strength between the metal and surrounding ligands. The greatest metal−ligand interaction was observed for the Os complexes, proceeding in the order Os > Ru > Ir > Rh. The higher bond strength of Os vs Ru has been modeled in other systems.[34]

To elucidate the reactivity difference between the Rh(III) species **6c** (pyridyl) and **7c** (triazolyl), the full reaction pathway was modeled using mechanistic features determined previously for the transformation of Cp*Rh species **A** into **B**. However, initially, **A** is electronically very different from **6c** and **7c**, being charge-neutral rather than cationic. Hypothesizing that the transformation of **6c** and **7c** relies on the formation of a metal−hydroxide species to evoke a combined proton−electron transfer step to afford the charge-neutral η^4-fulvene ligand, the generation of a vacant coordination site on the metal is necessary. For **A**, initially bearing two chlorido ligands, single Cl^{-} abstraction results in the well-stabilized mono-cationic chlorido−Rh(III) species **IIIc** that is able to accept the

Scheme 2. Reaction of 8′ with 1,3,5-Triaza-7-phosphaadamantane (pta)

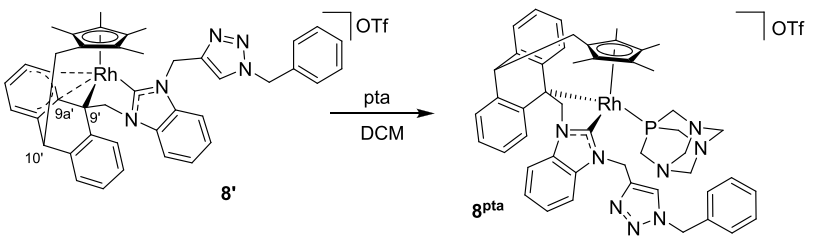

https://doi.org/10.1021/acsorginorgau.2c00035
ACS Org. Inorg. Au 2022, 2, 511−524

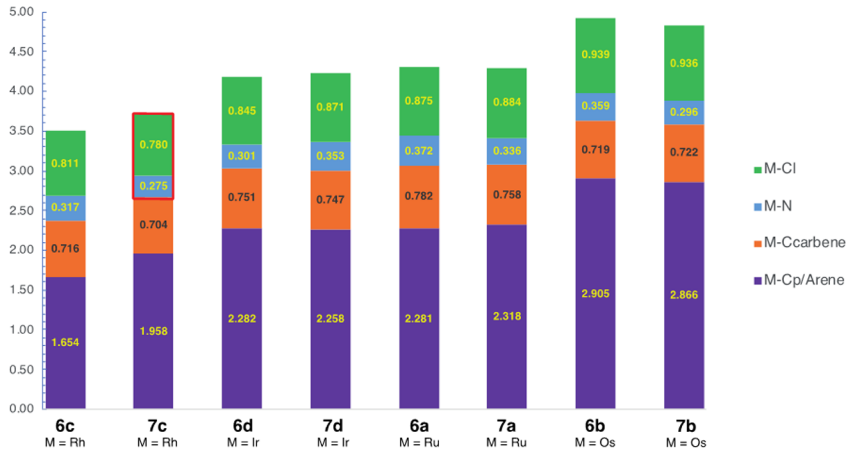

Figure 4. Comparison of the sum of the MBI values associated with the metal center for each complex. The weakest M−N and M−Cl bonds (highlighted by the red box) are associated with **7c**, the only complex in the series to undergo Cl^- abstraction and interligand coupling through metallo-cycloaddition affording complex **8′**.

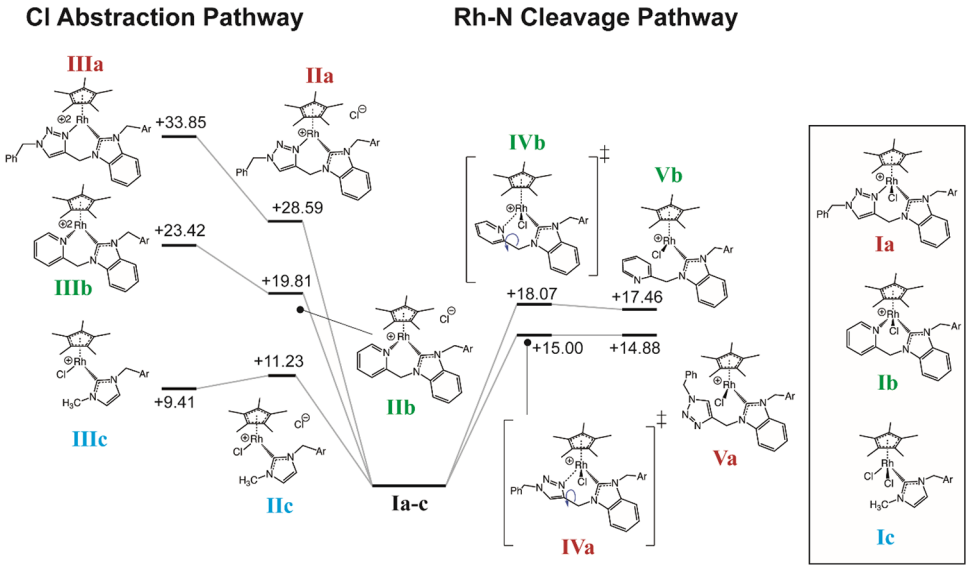

Figure 5. Two different DFT-calculated reaction pathways for generating a vacant metal coordination site on **Ia** and **Ib** for the incoming hydroxide anion (Ar = anthracenyl). For comparison, the previously reported Cl^- abstraction process for **Ic** is also shown and demonstrates the importance of a Rh−Cl bond present in the corresponding intermediate for stabilizing the resulting cationic Rh intermediate. All energies are solvent corrected (MeCN) and are reported in units of kcal mol^{-1}.

incoming OH^- group. In contrast, the ionization and generation of a dicationic Rh(III) species (**IIIa** and **IIIb**) from **6c** and **7c**, respectively, are not energetically favorable even if solvation helps to significantly lower the energy barrier (Figure 5, left). A geometry comparison between **IIc**/**IIIc** and **Ic** reveals that, in the latter, a planar alignment of the Rh, Cp*(centroid), C(carbene), and Cl is calculated, whereas in the dicationic complexes **IIc** and **IIIc**, a pyramidal arrangement is observed, presumably due to structural restrictions imposed by the chelating carbene-pyridyl/triazolyl ligand. Even if all systems maintain an approximately 86° bite angle, the metal−ligand orbital overlap is diminished, resulting in the unstable dicationic species **IIc** and **IIIc**. Hence, an alternative pathway (Figure 5, right) was envisaged whereby the stabilization of the Rh-bonded chloride was maintained while generating a vacant coordination site for the incoming hydroxide. This could be achieved by dissociation of the pyridyl or triazolyl pendant component rupturing the Rh−N bond through rotation of these planar groups along the methylene $C(H_2)$−C bond. In both cases, a transition state (**IVa**/**IVb**) was located leading to the partially dissociated species **Va** and **Vb** that are energetically less stable than **Ia** and **Ib** with an extremely low return energy barrier, which is suggestive of an equilibrium process, but significantly more stable than the corresponding solvated *N*-coordinated dicationic species **IIIb** and **IIIc**.

To rationalize the higher energy barrier associated with the pyridyl-based complex, a CM5 atomic charge (type IV) comparison (Figure 6) of the free ligands was conducted that indicates a significantly greater electron donation potential of N1 of the pyridyl group vs that on the triazolyl component, which also collaborates with the ability of the pyridyl component to better stabilize the dicationic complex **IIIb** than the triazolyl moiety in **IIIa**.

The full reaction pathway for the transformation of **Ia** and **Ib** into **XVIIIa** and **XVIIIb** is shown in Figure 7 (for more detailed diagrams, see the Supporting Information, Figures S10 and S11). It should be noted that only the transformation of **Ia** into **XVIIIb** is experimentally proposed, while there is no

https://doi.org/10.1021/acsorginorgau.2c00035
ACS Org. Inorg. Au 2022, 2, 511−524

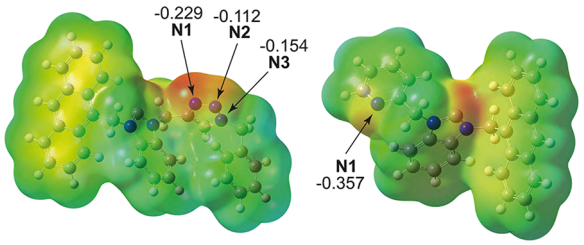

Figure 6. Comparison of DFT-calculated electrostatic potential maps and selected CM5 atom charges between the free triazolyl (left) and the pyridyl (right) carbene substituted anthracenyl-functionalized ligands. Both ligands were geometry-optimized to the minimum energy.

evidence for the formation of **XVIIIb** from **Ib**. Thus, starting with the pendant pyridyl/triazolyl N-dissociation from the Rh^{III} center (**Ia/b** → **IVa/b** → **Va/b**), the stabilized metal center accepts an incoming hydroxide ion, and the latter is an important substituent for the formation of the neutral η^4-fulvene ligand. Although hydroxide is not formally added as a salt during the syntheses of **6a/b** and **7a/b**, reaction conditions include the addition of Ag_2O. The formation of OH^- hence follows from the conversion of Ag_2O into Ag[OH], where silver oxide is known to be a strongly basic reagent.[35] Once the hydroxide has coordinated to the metal center to afford the combined Cl/OH substituted neutral species **VIIa** and **VIIb**, both of these species are identical with respect to the electronic configuration about the metal center. However, prior to the critical combined single electron-proton transfer (SEPT) step, loss of the chloride (**IXa/b**) and reattachment of the pendant donor group *via* N to the Rh center are required. Hence, the energy pathway of **VIIa/b** → **IXa/b** → **Xa/b** is almost identical except that rotation of the pendant triazolyl ring is slightly more favorable than that of the pyridyl ring. Surprisingly, once the Rh−N bond is re-established, the triazolyl-coordinated Rh−OH complex **XIa** is considerably more stable than the pendant pyridyl analog **XIb**, where MBI values indicate a stronger $Rh-N_{triazolyl}$ bond.

The next important step is the formation of the neutral fulvene ligand that is achieved by simultaneous abstraction of a proton from the methyl group from the capping Cp* ligand by the coordinated hydroxide, thus representing an inner sphere proton transfer process. This results in an exo-substituted ene functionality that represents a formal oxidation process. Concurrently, the Rh center is reduced from +3 to +1. Interestingly, the E_a barrier from **XIa/b** → **XIIa/b** is +24.27 and + 18.30 kcal mol^{-1} with SEPT more favorable for the triazolyl *N*-coordinated complex. The exo-ene functionality of the newly formed fulvene ligand, as previously observed during the transformation of complex **A**, does not bond with the metal center as observed for other Rh(I) species including the cationic $[\eta^4\text{-}(H_2C{=}C[C(H)C(H)]_2)Rh^I(PMe)_4]^+$ species reported by Hoard and Sharp.[36] Once water has formed as part of the transition states **XIIb** and **XIIc** and dissociated from the coordination sphere and the dispersion complexes **XIIIa** and **XIIIb** have broken down to form **XIVa** and **XIVb**, the final step of interligand coupling can proceed between the pendant anthracene and the exo-ene bond of the η^4-fulvene. This step relies on correctly aligning and positioning the anthracene group to be in close spatial proximity to the ene bond of the fulvene. Until this step, the lowest energy conformation of the anthracene is to be folded away (anti-conformation) from the C−Rh bond. However, the rotation of the anthracene plane along the C(ipso)−C(N) bond is facile, and the E_a barrier to reach the syn-conformation is very low (1.64 and 2.73 kcal mol^{-1}, respectively). With the pendant anthracene in the correct orientation (**XIIa/b** → **XIIIa/b** → **XIVa/b**), the spontaneous metallo-cycloaddition between the 9′- and 10′-carbon positions of anthracene and the Rh center and the exo-ene carbon atom of the η^4-fulvene proceeds to afford the transition states **XVIIa** and **XVIIb** with an E_a of +16.98 and +16.00 kcal mol^{-1}. During the cycloaddition, the Rh center is reoxidized back to a formal +3 state, and the aromaticity of the

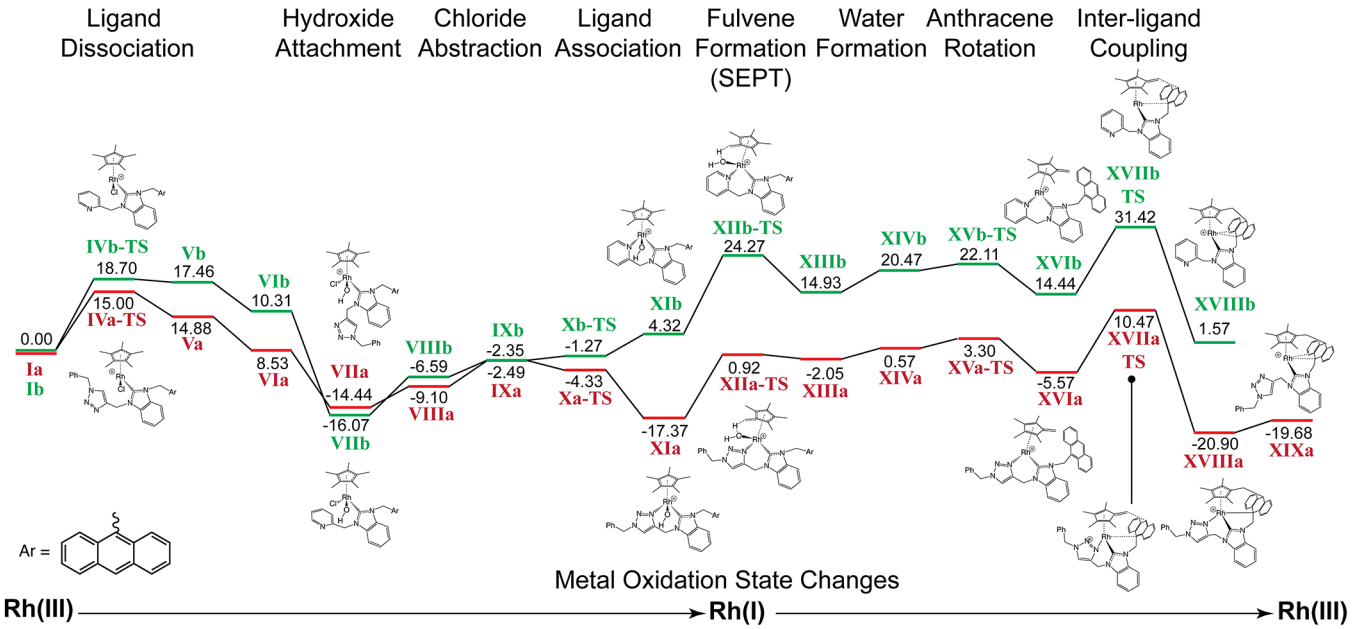

Figure 7. DFT (ω-B97xD/SMD(MeCN))-calculated reaction pathways for the conversion of **Ia** and **Ib** into **XVIIIa** and **XVIIIb**. Energies are given in kcal mol^{-1}. Only the conversion of **Ia** into **XIXa** is experimentally observed.

https://doi.org/10.1021/acsorginorgau.2c00035
ACS Org. Inorg. Au 2022, 2, 511−524

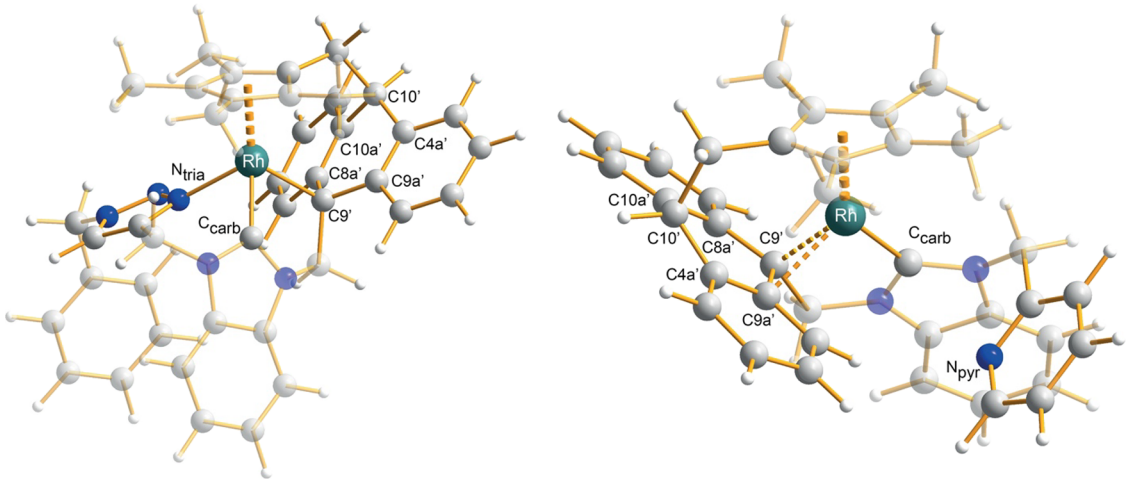

Figure 8. DFT calculated, geometry-optimized structures of **XVIIIa** (triazolyl, left) and **XVIIIb** (pyridyl, right) after interligand cycloaddition between the η^4-fulvene and anthracenyl substituent of the carbene ligand. Selected bond lengths: **XVIIIa**: Rh−C9′ 2.172 Å, C1−C10′ 1.571 Å; **XVIIIb**: Rh−C9′ 2.123 Å, Rh−C8a′ 2.242 Å, C1−C10′ 1.578 Å.

capping cyclopentadienyl group is restored. However, there is a significant difference in calculated geometry between the two types of Rh complexes. Specifically, during the cycloaddition process, the Rh−N distance for the pyridyl complex **VIIb** is extended to 3.811 Å, whereas in the triazole species **VIIa**, the Rh−N bond is 2.193 Å long and maintains covalent bonding with the metal center. Hence, the N atom of the pendant pyridyl group has become detached from the metal center and does not recoordinate in the final structure **XVIIIb**. In contrast, the triazolyl group maintains bonding to the Rh center during the cycloaddition process. Attempts to geometry-optimize an analog of **XVIIIb** whereby the N atom of the pendant pyridyl group is bonded to the Rh center were unsuccessful. Although molecular structures were not obtained for either **XVIIIa** or **XVIIIb**, solution NMR evidence indicates that only species **XIXa** is experimentally observable, while **XVIIIb** is only theoretically proposed. The structures of the DFT-modeled cationic complexes are shown in Figure 8.

There are few notable structural differences between the two final cationic species. One significant difference is the coordination of the pendant triazolyl in **XVIIIa** and the uncoordinated pyridyl in **XVIIIb** with the full rationale discussed in the Supporting Information. The presence of a Rh−N bond has a strong influence on the metal−anthracenyl interaction. For the triazolyl complex with a Rh−N bond, a single C−C bond (1.571 Å) bridges the substituted cyclopentadienyl group, along with a single Rh−C bond with a length of 2.172 Å in which the MBI indicates a relatively strong bond (Figure S12). In contrast, for the pyridyl complex, the lack of the Rh−N bond has increased the Lewis acidity of the metal center, and thus, a stronger Rh interaction with the anthracenyl group is calculated with two Rh−C covalent bonds (Rh and C9′/C8a′, Figure S12). The covalent nature of this η^2-anthracenyl bonding was confirmed by analysis of the reduced electron density gradient using the Interaction Region Indicator (IRI) methodology (Figure S13). This unusual, seemingly pseudo-nonadentate bonding interaction is analogous to that described previously for complex **B**.[28]

Electronic absorption and fluorescence emission spectra of the pro-carbenes (**4**, **5**) and anthracenyl-functionalized NHC-pyridyl (**6a−d**) and -triazolyl (**7a−d**, **8′**) complexes were recorded in methanol. The pro-carbenes **4** and **5** and their complexes **6a−d** and **7a−d** showed UV−vis spectra with absorption maxima arising mainly from the anthracenyl moieties at *ca.* 360 nm (Figure S14), which demonstrate the typical vibronic coupling associated with this functional group. However, a very different absorption spectrum with a broad band at 570 nm was observed for complex **8′** where the vibronic coupling is lost due to C−C bond formation between the anthracenyl and Cp* moieties and the loss of aromaticity of the central anthracene ring (Figure S14). However, it appears that the experimental spectrum features two related species as band B is divided into two peaks. Employing time-dependent DFT modeling with solvent corrections for methanol, two separate spectra were calculated for complex **8**, one with pendant triazolyl coordinated (**8**) and the other without triazolyl coordination (**8′**; Figures S15 and S16). The calculations reproduced the three main bands (A−C) observed in the experimental spectrum and suggest that an equilibrium between pendant triazolyl coordination and dissociation with the Rh center occurs in solution. A significant difference between the two calculated spectra is the absence of band C in the case of Rh-triazolyl coordinated **8**. An MO analysis of the electronic structure within **8** and **8′** revealed that the absence of a Rh−N bond in **8′** significantly reduces the HOMO−LUMO energy gap (6.41 vs 7.27 eV in **8**), enabling a lower energy LMCT (Figure S16). A complete description of the bonding structure in **8** and **8′** using charge decomposition analysis (CDA) is given in the Supporting Information (Figures S17 and S18).

Typical fluorescence spectra for anthracenyl-containing molecules were observed in both series of compounds (Figure S19).[27] The emission maxima were very similar for the pro-carbenes **4** and **5** with two main features at about 396 and 417 nm. Upon metal coordination in **6a−d** and **7a−d**, the maxima shift very slightly to lower wavelengths, and the latter peaks decreased markedly in intensity compared to the bands at about 396 nm relative to the spectra of the pro-carbenes. In the case of **8′**, the band at 392 nm was significantly more pronounced and shifted to a lower wavelength than in **7c** and the other complexes (Figure S19 and Table S5). Given the change in structure to the anthracenyl unit upon C−C bond formation and coordination to the Rh center, it would be

https://doi.org/10.1021/acsorginorgau.2c00035
ACS Org. Inorg. Au 2022, 2, 511−524

expected that the vibronic coupling is lost in both the absorbance and fluorescence spectra.

CONCLUSIONS

A series of monocationic $M^{II/III}$(cym/Cp*) complexes (M = Ru, Os, Rh, and Ir) featuring an anthracenyl-substituted NHC ligand bearing a pendant pyridyl or triazolyl moieties was prepared and characterized. Interestingly, only in the case of the (Cp*)Rh complex bearing the triazolyl group was a new polydentate ligand formed *in situ via* C−C bond formation between the fulvene group, which was formed *via* deprotonation of a methyl group of the Cp* ligand, and the pendant anthracenyl group for **7c**. This species presents with unusual bonding properties similar to those previously reported for the neutral Rh species **B**. The NMR spectroscopic data indicate the formation of the organorhodium compound **8** featuring an octadentate ligand with seven carbon and one nitrogen centers coordinated to the Rh center (**8**), while the analogous pyridyl-substituted Rh complex **6c** did not undergo the same internal ligand transformation. Proposed reaction pathways for the transformation of complexes **6c** and **7c** were DFT-calculated with parts of the mechanism based on the previously described conversion of **A** into **B**, except that the metal coordination lability of pendant N-donor groups was considered. Overall, DFT calculations suggest that **7c** has a lower energy pathway for the conversion process, whereby proton extraction is accompanied by metal reduction and reoxidation upon the formation of new C−C and Rh−C bonds. This is consistent with experimental observations for the preparation of complex **8′** from **7c**. Moreover, the MBI values correlate with this finding as the weakest Rh−Cl and Rh−N bonds of the metal complex series are associated with the triazolyl species **7c**. Moreover, the pendant triazolyl N−metal coordination in the final complex **8** is shown to be highly labile, as the metal uncoordinated species **8′** is only +1.01 kcal/mol higher in energy. UV−visible absorption spectroscopy data for **8** were largely consistent with spectra calculated with TD-DFT. However, the absorption spectrum featured a characteristic shoulder that is suggested by theory upon dissociation of the triazolyl moiety as found in **8′**. The minor energy difference between **8** and **8′** and the absence of vibronic coupling in the fluorescence spectrum of **8′** suggest the formation of an equilibrium interconversion process between two species in solution. This was also supported by reactivity studies of **8′** and pta that revealed that indeed the Rh−C bond to the anthracenyl-derived ligand is weak and is easily replaced by a stronger electron donor. Finally, a CDA of calculated DFT models of **8** and **8′** indicates that the former contains a single octadentate ligand with weak Rh−$N_{triazolyl}$ bonding. Species **8′** features no Rh−$N_{triazolyl}$ bond but instead has an asymmetric pseudo-allylic η^3-interaction between the π-system of the transformed anthracenyl group; thus, the single ligand in **8′** is formally considered to feature a highly unusual and a rare case of nonadenticity.

EXPERIMENTAL SECTION

Materials and Methods

All reactions were carried out under a nitrogen atmosphere using standard Schlenk techniques. When the reactions required heating, oil baths on stirrer hotplates were used. Chemicals obtained from commercial suppliers were used as received and were analytical grade. Methanol (Macron, AR) and tetrahydrofuran (J.T. Baker, AR) were dried over activated molecular sieves (3 Å) in round-bottom flasks for 2 days prior to use. Acetonitrile and dichloromethane were purchased from J.T. Baker; ethylacetate was from Macron; and 9-chloromethylanthracene, benzimidazole, silver triflate, and 2-(bromomethyl)-pyridine were from AK Scientific. Copper sulfate pentahydrate (98%), *n*-hexane, potassium hydroxide, and sodium sulfate anhydrous (98%) were purchased from ECP; propargyl bromide (80 wt % in toluene) was from Aldrich; and ammonium hexafluorophosphate (99.5%) was from Acros Organic. Silver hexafluorophosphate, celite, 1,2,3,4,5-pentamethylcyclopentadiene, silver(I) oxide (99%), sodium L-ascorbate (98%), *tert*-butanol, benzyl azide, and α-terpinene (89%) were supplied by Sigma-Aldrich. Osmium(III) chloride hydrate (55% metal content) was from Heraeus South Africa, whereas ruthenium(III) chloride hydrate (99%), rhodium(III) chloride hydrate (99%), and iridium(III) chloride hydrate (99%) were from Precious Metals Online. The dimeric precursors $[M^{II/III}(cym/Cp^*)Cl_2]_2$ (M = Ru, Os, Rh, Ir) were synthesized by adapting literature procedures.[37,38]

^{1}H and ^{13}C{^{1}H} and 2D (COSY, HSQC, HMBC) NMR spectra were recorded on a Bruker Avance AVIII 400 MHz NMR spectrometer at ambient temperature at 400.13 (^{1}H), 100.61 (^{13}C{^{1}H}), or 161.87 MHz (^{31}P{^{1}H}). Chemical shifts are reported vs $SiMe_4$ and were determined by reference to the residual solvent peaks. Mass spectra were recorded on a Bruker micrOTOF-QII mass spectrometer in positive electrospray ionization (ESI) mode. Elemental analyses were conducted on a Vario EL cube (Elementar Analysensysteme GmbH, Hanau, Germany).

X-ray diffraction measurements of single crystals of **4** and **6a** were performed on a Rigaku Oxford Diffraction XtaLAB-Synergy-S single-crystal diffractometer with a PILATUS 200K hybrid pixel array detector using Cu Kα radiation (λ = 1.54184 Å; Table S6). The data were processed with the SHELXT and Olex2 1.3 software packages.[39−41] All nonhydrogen atoms were refined anisotropically. Hydrogen atoms were inserted at calculated positions and refined with a riding model or without restrictions. Mercury 2020.3 was used to visualize the molecular structures. A SHIMADZU UV-3600 Plus spectrophotometer was used to record the UV−vis spectra and a JASCO FP-8600 NIR spectrofluorometer for the fluorescence emission spectra.

Synthesis of 1-(Pyridin-2-ylmethyl)benzimidazole, 1.

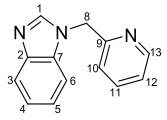

Benzimidazole (0.47 g, 40 mmol, 1 equiv) and 2-(bromomethyl)-pyridine (1.00 g, 40 mmol, 1 equiv) were dissolved in tetrahydrofuran (30 mL). Potassium hydroxide (0.89 g, 158 mmol, 4 equiv) was added to the mixture that was refluxed for 48 h.[8] The solution was filtered, and the solvent was removed under reduced pressure. The yellow residue was dissolved in dichloromethane (DCM), and the DCM solution was washed with water. The organic phase was then dried with anhydrous sodium sulfate and filtered. The solvent was removed under reduced pressure to afford a yellow solid. Yield: 747 mg (89%). ^{1}H NMR (400.13 MHz, DMSO-d_6): δ (ppm) = 8.51−8.52 (m, 1H, H13), 8.37 (s, 1H, H1), 7.77 (td,^3J = 8 Hz,^4J = 2 Hz, 1H, H11), 7.63−7.68 (m, 1H, H3), 7.45−7.50 (m, 1H, H6), 7.26−7.31 (m, 2H, H10, H12), 7.15−7.21 (m, 2H, H4, H5), 5.59 (s, 2H, H8).

Synthesis of (9-Anthracenylmethyl)benzimidazole, 2.

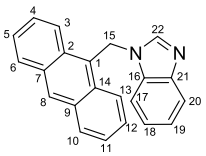

A mixture of 9-chloromethylanthracene (0.348 g, 2.94 mmol, 1 equiv), benzimidazole (0.668 g, 2.94 mmol, 1 equiv), and potassium hydroxide (0.661 g, 11.8 mmol, 4 equiv) in 60 mL THF was refluxed in darkness for 2 days under nitrogen. The solvent was removed under vacuum. The red residue was extracted with DCM, then sodium sulfate was added, and the solution was filtered and evaporated to

https://doi.org/10.1021/acsorginorgau.2c00035
ACS Org. Inorg. Au 2022, 2, 511−524

afford a pale brown solid. Yield: 0.850 g (94%). ^{1}H NMR (400.13 MHz, $CDCl_3$): δ (ppm) = 8.63 (s, 1H, H22), 8.29−8.35 (m, 1H, H8), 8.08−8.14 (m, 4H, H3, H6, H10, H13), 7.81−7.84 (m, 1H, H17), 7.70−7.73 (m, 1H, H20), 7.49−7.55 (m, 4H, H4, H5, H11, H12), 7.45 (dt, ^3J = 7 Hz,^4J = 1 Hz, 1H, H18), 7.36 (dt,^3J = 7 Hz,^4J = 1 Hz, 1H, H19), 6.19 (s, 2H, H15).

Synthesis of 1-(Anthracen-9-ylmethyl)-3-(prop-2-yn-1-yl)-benzimidazolium Bromide, 3.

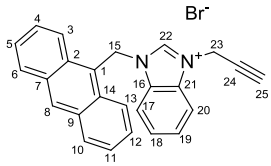

A mixture of 1-(9-anthracenylmethyl)-1*H*-benzimidazole (850 mg, 2.76 mmol, 1.00 equiv) and propargyl bromide (409 mg, 3.45 mmol, 1.25 equiv) in acetonitrile was refluxed in darkness for 3 days under nitrogen. The solvent was evaporated under reduced pressure. Ethylacetate was added to the residue, the resultant suspension was filtered, and the solvent was evaporated to afford a brown solid. Yield: 622 mg (53%). ^{1}H NMR (400.13 MHz, DMSO-d_6): δ (ppm) = 8.99 (s, 1H, H22), 8.93 (s, 1H, H8), 8.35−8.42 (m, 3H, H3/H6/H10/H13/H17/H20), 8.25−8.29 (m, 2H, H3/H6/H10/H13), 8.04−8.08 (m, 1H, H17/H20), 7.79−7.88 (m, 2H, H18, H19), 7.61−7.68 (m, 4H, H4, H5, H11, H12), 6.74 (s, 2H, H15), 5.28 (d,^3J = 3 Hz, 2H, H23), 3.69 (t,^2J = 3 Hz, 1H, H25). MS (ESI$^+$) *m*/*z*: $[M - Br]^+$ calculated for $C_{25}H_{19}N_2$ 347.1543; found 347.1530.

Synthesis of 1-(Anthracen-9-ylmethyl)-3-(pyridin-2-ylmethyl)benzimidazolium Hexafluorophosphate, 4.

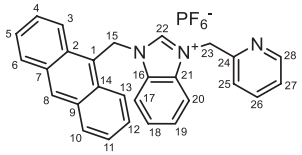

A mixture of **1** (0.69 g, 3.3 mmol, 1 equiv), 9-chloromethylanthracene (0.75 g, 3.3 mmol, 1 equiv), and NH_4PF_6 (1.1 g, 6.6 mmol, 2 equiv) in 50 mL acetonitrile was refluxed for 2 days under nitrogen, resulting in the formation of a yellow precipitate. The precipitate was filtered, washed with ethyl acetate, and dried under a vacuum to afford a yellow solid. Yield: 779 mg (60%). Single crystals suitable for X-ray diffraction analysis were grown from deuterated chloroform. ^{1}H NMR (400.13 MHz, DMSO-d_6): δ (ppm) = 9.22 (s, 1H, H22), 8.92 (s, 1H, H8), 8.42 (d,^3J = 8 Hz, 2H, H3/H6/H10/H13), 8.26−8.32 (m, 4H, H3/H6/H10/H13/H17/H20/H28), 7.91 (d,^3J = 8 Hz, 1H, H17/H20), 7.74−7.82 (m, 2H, H18/H19/H27), 7.61−7.70 (m, 5H, H4/H5/H11/H12/H18/H19), 7.45 (d,^3J = 8 Hz, 1H, H25), 7.29 (dd,^3J = 5 Hz,^4J = 1 Hz, 1H, H26), 6.81 (s, 2H, H15), 5.73 (s, 2H, H23). ^{13}C{^{1}H} NMR (100.61 MHz, DMSO-d_6): δ (ppm) = 152.9 (C, C24), 149.3 (CH, C28), 142.3 (CH, C22), 137.4 (CH, C27), 131.7 (C, C2/C7/C9/C14), 131.6 (C, C2/C7/C9/C14), 131.2 (C, 2C, C16, C21), 131.1 (C, 2C , C2/C7/C9/C14), 130.5 (CH, C8), 129.5 (CH, 2C, C3/C6/C10/C13), 127.8 (CH, C4/C5/C11/C12), 127.0 (CH, C18/C19), 126.7 (CH, C18/C19), 125.7 (CH, C4/C5/C11/C12), 123.5 (CH, C26), 123.4 (CH, 2C, C3/C6/C10/C13), 122.2 (CH, C25), 121.9 (C, C1), 114.4 (CH, C17/C20), 113.9 (CH, C17/C20), 50.6 (NCH_2, C15), 43.6 (NCH_2, C23). MS (ESI$^+$) *m*/*z*: $[M - PF_6]^+$ calculated for $C_{28}H_{22}N_3$ 400.1808; found 400.1811.

Synthesis of 1-(Anthracen-9-ylmethyl)-3-((1-benzyl-1,2,3-triazol-4-yl)methyl)benzimidazolium Hexafluorophosphate, 5.

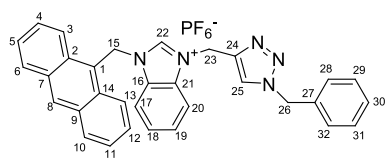

Copper sulfate (18 mg, 0.07 mmol, 0.1 equiv) and sodium ascorbate (56 mg, 0.28 mmol, 0.4 equiv) were dissolved in water (20 mL). A solution of **3** (300 mg, 0.70 mmol, 1.0 equiv) in a mixture of *tert*-butanol (80 mL)/water (20 mL) and benzyl azide (103 mg, 0.77 mmol, 1.1 equiv) was added. The reaction mixture was refluxed in darkness for 3 days under nitrogen. NH_4PF_6 (515 mg, 3.16 mmol, 4.5 equiv) was added to the reaction mixture and refluxed for 1 day. The solvents were removed under vacuum. Dichloromethane was added to the brown residue, the resultant suspension was filtered, and the solvent was evaporated to afford a pale brown solid. Yield: 327 mg (75%). ^{1}H NMR (400.13 MHz, DMSO-d_6): δ (ppm) = 9.16 (s, 1H, H22), 8.93 (s, 1H, H8), 8.37−8.38 (m, 2H, H3/H6/H10/H13), 8.29−8.32 (d,^3J = 8 Hz, 1H, H17/H20), 8.25−8.29 (m, 2H, H3/H6/H10/H13), 8.18 (s, 1H, H25), 8.05 (d,^3J = 8 Hz, 1H, H17/H20), 7.71−7.81 (m, 2H, H18, H19), 7.61−7.65 (m, 4H, H4, H5, H11, H12), 7.31−7.37 (m, 3H, H28/H29/H30/H31/H32), 7.22−7.24 (m, 2H, H28/H29/H30/H31/H32), 6.73 (s, 2H, H15), 5.65 (s, 1H, H26), 5.55 (s, 1H, H23). ^{13}C{^{1}H} NMR (100.61 MHz, DMSO-d_6): δ (ppm) = 141.4 (CH, C22), 140.4 (C, C24), 135.7 (C, C27), 131.8 (C, C2/C7/C9/C14), 131.2 (C, 2C, C16, C21), 131.1 (C, C2/C7/C9/C14), 131.0 (C, 2C, C2/C7/C9/C14), 130.6 (CH, C8), 129.5 (CH, 2C, C3/C6/C10/C13), 128.7 (CH, 2C, C28/C29/C30/C31/C32), 128.2 (CH, C28/C29/C30/C31/C32), 127.9 (CH, 2C, C28/C29/C30/C31/C32), 127.8 (CH, 2C, C4/C5/C11/C12), 126.9 (CH, C18/C19), 126.8 (CH, C18/C19), 125.7 (CH, 2C, C4/C5/C11/C12), 124.5 (CH, C25), 123.4 (CH, 2C, C3/C6/C10/C13), 121.8 (C, C1), 114.4 (CH, C17/C20), 114.1 (CH, C17/C20), 52.9 (NCH_2, C26), 43.5 (NCH_2, C15), 41.6 (NCH_2, C23). MS (ESI$^+$) *m*/*z*: $[M - PF_6]^+$ calculated for $C_{32}H_{26}N_5$ 480.2183; found 480.2178.

General Procedure for the Synthesis of Pyridyl-Functionalized NHC−M(cym/Cp*) Complexes

Compound **4** was dissolved in acetonitrile (20 mL) and methanol (0.2 mL), silver oxide was added to the solution, and the mixture was refluxed in darkness for 72 h under nitrogen. A solution of $[M^{II/III}(cym/Cp^*)Cl_2]_2$ in acetonitrile (5 mL) was added to the reaction mixture that was then refluxed for 24 h. Then a solution of NH_4PF_6 or $AgPF_6$ in acetonitrile (5 mL) was added to the reaction mixture, and the mixture was refluxed for 24 h. The resultant suspension was filtered over Celite, and the filtrate was collected and evaporated under reduced pressure. The residue was dissolved in a minimal volume of dichloromethane (*ca.* 1 mL), and *n*-hexane was added to the solution, which led to the immediate formation of an orange precipitate. The precipitate was filtered, washed with *n*-hexane, and dried under vacuum to afford complexes **6a**−**6d**.

Synthesis of {Chlorido[1-(anthracen-9-ylmethyl)-3-(pyridin-2-ylmethyl-*κN*)benzimidazol-2-ylidene-*κC*](*η*^{6}-*p*-cymene)-ruthenium(II)} Hexafluorophosphate, 6a.

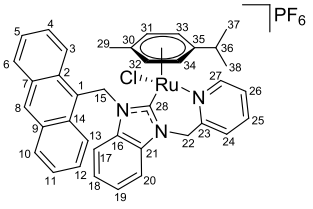

Compound **6a** was prepared by following the general procedure using **4** (50 mg, 0.11 mmol, 2.0 equiv), silver oxide (20 mg, 0.09 mmol, 1.5 equiv), $[Ru(cym)Cl_2]_2$ (35 mg, 0.06 mmol, 1.0 equiv), and NH_4PF_6 (93 mg, 0.57 mmol, 10 equiv). Yield: 30 mg (32%). Single crystals suitable for X-ray diffraction analysis were grown from deuterated chloroform. ^{1}H NMR (400.13 MHz, $CDCl_3$): δ (ppm) = 9.26 (dd,^3J = 6 Hz,^4J = 1 Hz, 1H, H27), 8.65 (s, 1H, H8), 8.41 (m, 1H, H3/H4/H5/H6/H10/H11/H12/H13), 8.04−8.10 (m, 3H, H3/H4/H5/H6/H10/H11/H12/H13), 7.91 (td,^3J = 8 Hz,^4J = 1 Hz, 1H, H26), 7.79 (d,^3J = 8 Hz, 1H, H24), 7.58 (d,^3J = 8 Hz, 1H, H17/H20), 7.45−7.56 (m, 3H, H3/H4/H5/H6/H10/H11/H12/H13), 7.39−7.44 (m, 2H, H3/H4/H5/H6/H10/H11/H12/H13, H25), 7.09−7.16 (m, 2H, H15, H18/H19), 6.59−6.65 (m, 2H, H15, H18/H19), 5.76−5.83 (m, 3H, H17/H20, H22, H31/H32/H33/H34), 5.62 (dd,^3J = 6 Hz, 1H, H31/H32/H33/H34), 5.56 (dd,^3J = 6 Hz, 1H, H31/H32/H33/H34), 5.54 (dd,^3J = 6 Hz, 1H, H31/H32/H33/H34), 5.28 (d,^2J = 16

https://doi.org/10.1021/acsorginorgau.2c00035
ACS Org. Inorg. Au 2022, 2, 511−524

Hz, 1H, H22), 2.96 (sept,^3J = 7 Hz, 1H, H36), 2.23 (s, 3H, H29), 1.25 (d,^3J = 7 Hz, 3H, H37/H38), 1.23 (d,^3J = 7 Hz, 3H, H37/H38). $^{13}C\{^1H\}$ NMR (100.61 MHz, $CDCl_3$): δ (ppm) = 188.4 (C, C28), 157.7 (CH, C27), 156.3 (C, C23), 139.8 (CH, C26), 134.9 (C, C16/C21), 134.0 (C, C16/C21), 131.4 (C, 4C, C2, C7, C9, C14), 129.9 (CH, 2C, C3/C4/C5/C6/C8/C10/C11/C12/C13), 129.2 (CH, C3/C4/C5/C6/C10/C11/C12/C13), 127.5 (CH, 2C, C3/C4/C5/C6/C10/C11/C12/C13), 126.1 (CH, C24), 125.7 (CH, C3/C4/C5/C6/C10/C11/C12/C13), 125.5 (CH, C3/C4/C5/C6/C10/C11/C12/C13), 124.8 (CH, C25), 124.2 (C, C1), 123.9 (CH, C3/C4/C5/C6/C10/C11/C12/C13), 123.8 (CH, C18/C19), 123.7 (CH, C18/C19), 122.8 (CH, C3/C4/C5/C6/C10/C11/C12/C13), 113.9 (C, C30/C35), 111.9 (CH, C17/C20), 110.0 (CH, C17/C20), 101.8 (C, C30/C35), 88.8 (CH, C31/C32/C33/C34), 87.9 (CH, C31/C32/C33/C34), 85.6 (CH, C31/C32/C33/C34), 85.1 (CH, C31/C32/C33/C34), 51.5 (NCH_2, C22), 48.6 (NCH_2, C15), 31.4 (CH, C36), 23.8 (CH_3, C37/C38), 21.1 (CH_3, C37/C38), 18.8 (CH_3, C29). MS (ESI^+) m/z: $[M - PF_6]^+$ calculated for $C_{38}H_{35}ClN_3Ru$ 670.1565; found 670.1573. Elemental analysis calculated for $C_{38}H_{35}ClN_3RuPF_6$: C 55.99, H 4.33, N 5.15%; found: C 55.61, H 4.70, N 4.81%.

Synthesis of {Chlorido[1-(anthracen-9-ylmethyl)-3-(pyridin-2-ylmethyl-κN)benzimidazol-2-ylidene-κC](η^6-*p*-cymene)-osmium(II)} Hexafluorophosphate, 6b.

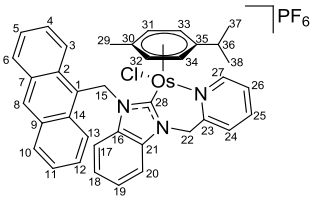

Compound **6b** was prepared by following the general procedure using **4** (100 mg, 0.23 mmol, 2.0 equiv), silver oxide (40 mg, 0.17 mmol, 1.5 equiv), $[Os(cym)Cl_2]_2$ (91 mg, 0.11 mmol, 1.0 equiv), and NH_4PF_6 (187 mg, 1.1 mmol, 10 equiv). Yield: 49 mg (24%). ^1H NMR (400.13 MHz, $CDCl_3$): δ (ppm) = 9.09 (d,^3J = 6 Hz, 1H, H27), 8.65 (s, 1H, H8), 8.34−8.47 (m, 1H, H3/H4/H5/H6/H10/H11/H12/H13), 8.02−8.18 (m, 3H, H3/H4/H5/H6/H10/H11/H12/H13), 7.84−7.90 (m, 2H, H24, H26), 7.59 (d,^3J = 8 Hz, 1H, H17/H20), 7.43−7.55 (m, 4H, H3/H4/H5/H6/H10/H11/H12/H13), 7.34 (t,^3J = 6 Hz, 1H, H25), 7.07−7.14 (m, 2H, H15, H18/H19), 6.55−6.62 (m, 2H, H15, H18/H19), 5.86 (d,^2J = 16 Hz, 1H, H22), 5.81 (d,^3J = 6 Hz, 1H, H31/H32/H33/H34), 5.76 (d,^3J = 8 Hz, 1H, H17/H20), 5.65−5.73 (m, 3H, H31/H32/H33/H34), 5.25 (d,^2J = 16 Hz, 1H, H22), 2.90 (sept,^3J = 7 Hz, 1H, H36), 2.36 (s, 3H, H29), 1.28 (d,^3J = 7 Hz, 3H, H37/H38), 1.21 (d,^3J = 7 Hz, 3H, H37/H38). $^{13}C\{^1H\}$ NMR (100.61 MHz, $CDCl_3$): δ (ppm) = 172.7 (C, C28), 157.8 (CH, C27), 155.3 (C, C23), 140.2 (CH, C26), 134.6 (C, C16/C21), 133.4 (C, C16/C21), 129.9 (CH, 2C, C3/C4/C5/C6/C8/C10/C11/C12/C13), 129.2 (CH, C3/C4/C5/C6/C10/C11/C12/C13), 127.5 (CH, 2C, C3/C4/C5/C6/C10/C11/C12/C13), 125.6 (CH, 2C, C24, C3/C4/C5/C6/C10/C11/C12/C13), 125.2 (CH, 2C, C25, C3/C4/C5/C6/C10/C11/C12/C13), 124.4 (CH, C3/C4/C5/C6/C10/C11/C12/C13), 124.3 (C, C1), 123.9 (CH, C18/C19), 123.8 (CH, C18/C19), 123.2 (CH, C3/C4/C5/C6/C10/C11/C12/C13), 111.9 (CH, C17/C20), 110.3 (CH, C17/C20), 104.8 (C, C30/C35), 93.9 (C, C30/C35), 80.3 (CH, C31/C32/C33/C34), 79.5 (CH, C31/C32/C33/C34), 76.5 (CH, C31/C32/C33/C34), 76.2 (CH, C31/C32/C33/C34), 52.0 ($C(H_2)$−N, C22), 48.6 ($C(H_2)$−N, C15), 31.3 (CH, C36), 24.4 (CH_3, C37/C38), 21.1 (CH_3, C37/C38), 18.7 (CH_3, C29). MS (ESI^+) m/z: $[M - PF_6]^+$ calculated for $C_{38}H_{35}ClN_3Os$ 760.2120; found 760.2147. Elemental analysis calculated for $C_{38}H_{35}ClN_3OsPF_6 \cdot 1.9\ H_2O \cdot 1.6\ CH_2Cl_2$: C 44.27, H 3.94, N 3.91%; found: C 44.06, H 3.97, N 4.15%.

Synthesis of {Chlorido[1-(anthracen-9-ylmethyl)-3-(pyridin-2-ylmethyl-κN)benzimidazol-2-ylidene-κC](η^5-pentamethylcyclopentadienyl)rhodium(III)} Hexafluorophosphate, 6c.

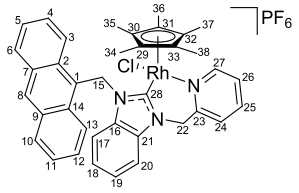

Compound **6c** was prepared by following the general procedure using **4** (50 mg, 0.11 mmol, 2.0 equiv), silver oxide (20 mg, 0.08 mmol, 1.5 equiv), $[Rh(Cp^*)Cl_2]_2$ (35 mg, 0.06 mmol, 1.0 equiv), and $AgPF_6$ (29 mg, 0.11 mmol, 2.0 equiv). Yield: 38 mg (40%). ^1H NMR (400.13 MHz, $CDCl_3$): δ (ppm) = 9.03 (d,^3J = 6 Hz, 1H, H27), 8.66 (s, 1H, H8), 8.38 (d,^3J = 9 Hz, 1H, H3/H4/H5/H6/H10/H11/H12/H13), 8.16 (m, 2H, H3/H4/H5/H6/H10/H11/H12/H13), 8.00−8.04 (m, 3H, H3/H4/H5/H6/H10/H11/H12/H13, H25, H26), 7.71 (d,^3J = 8 Hz, 1H, H17/H20), 7.53−7.61 (m, 3H, H3/H4/H5/H6/H10/H11/H12/H13, H24), 7.47 (d,^2J = 14 Hz, 1H, H15), 7.39−7.43 (m, 1H, H3/H4/H5/H6/H10/H11/H12/H13), 7.28−7.32 (m, 1H, H3/H4/H5/H6/H10/H11/H12/H13), 7.08 (td,^3J = 8 Hz,^4J = 1 Hz, 1H, H18/H19), 6.47 (td,^3J = 8 Hz,^4J = 1 Hz, 1H, H18/H19), 6.36 (d,^2J = 14 Hz, 1H, H15), 6.01 (d,^2J = 16 Hz, 1H, H22), 5.36 (d,^3J = 8 Hz, 1H, H17/H20), 5.25 (d,^2J = 16 Hz, 1H, H22), 1.82 (s, 15H, Cp*). $^{13}C\{^1H\}$ NMR (100.61 MHz, $CDCl_3$): δ (ppm) = 181.8 (d,^1J = 51 Hz, C , C28), 155.5 (CH, C27), 155.4 (C, C23), 140.4 (CH, C26), 134.6 (C, C16), 134.3 (C, C21), 132.3 (C, C2/C7/C9/C14), 131.7 (C, C2/C7/C9/C14), 131.3 (C, C2/C7/C9/C14), 131.2 (C, C2/C7/C9/C14), 130.1 (CH, H8), 130.0 (CH, C3/C4/C5/C6/C10/C11/C12/C13), 128.9 (CH, C3/C4/C5/C6/C10/C11/C12/C13), 127.8 (CH, C3/C4/C5/C6/C10/C11/C12/C13), 127.5 (CH, C3/C4/C5/C6/C10/C11/C12/C13), 126.8 (CH, C25), 126.1 (CH, C24), 125.8 (CH, C3/C4/C5/C6/C10/C11/C12/C13), 125.3 (CH, C3/C4/C5/C6/C10/C11/C12/C13), 124.9 (CH, C3/C4/C5/C6/C10/C11/C12/C13), 124.0 (CH, C18/C19), 123.9 (CH, C18/C19), 123.4 (C, C1), 122.5 (CH, C3/C4/C5/C6/C10/C11/C12/C13), 112.2 (CH, C17/C20), 110.8 (CH, C17/C20), 99.4 (d,^1J = 7 Hz, C, Cp*), 50.9 (NCH_2, C22), 48.3 (NCH_2, C15), 9.9 (CH_3, Cp*). MS (ESI^+) m/z: $[M - PF_6]^+$ calculated for $C_{38}H_{36}ClN_3Rh$ 672.1649; found 672.1639. Elemental analysis calculated for $C_{38}H_{36}ClN_3RhPF_6 \cdot 0.1\ H_2O \cdot 0.08\ C_6H_{14}$: C 55.9, H 4.55, N 5.08%; found: C 55.7, H 4.91, N 5.44%.

Synthesis of {Chlorido[1-(anthracen-9-ylmethyl)-3-(pyridin-2-ylmethyl-κN)benzimidazol-2-ylidene-κC](η^5-pentamethylcyclopentadienyl)iridium(III)} Hexafluorophosphate, 6d.

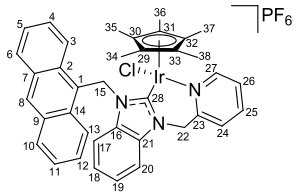

Compound **6d** was prepared by following the general procedure using **4** (50 mg, 0.11 mmol, 2.0 equiv), silver oxide (20 mg, 0.08 mmol, 1.5 equiv), $[Ir(Cp^*)Cl_2]_2$ (46 mg, 0.06 mmol, 1.0 equiv), and NH_4PF_6 (47 mg, 0.29 mmol, 5.0 equiv). Yield: 44 mg (42%). ^1H NMR (400.13 MHz, $CDCl_3$): δ (ppm) = 8.96 (dd,^3J = 6 Hz,^4J = 1 Hz, 1H, H27), 8.66 (s, 1H, H8), 8.40 (d,^3J = 8 Hz, 1H, H3/H4/H5/H6/H10/H11/H12/H13), 8.15 (d,^3J = 8 Hz, 1H, H3/H4/H5/H6/H10/H11/H12/H13), 8.13 (d,^3J = 8 Hz, 1H, H3/H4/H5/H6/H10/H11/H12/H13), 8.02−8.04 (m, 2H, H3/H4/H5/H6/H10/H11/H12/H13, H25), 7.98 (td,^3J = 8 Hz,^4J = 1 Hz, 1H, H26), 7.71 (d,^3J = 8 Hz, 1H, H17/H20), 7.49−7.60 (m, 3H, H3/H4/H5/H6/H10/H11/H12/H13, H24), 7.42 (d,^2J = 14 Hz, 1H, H15), 7.40 (td,^3J = 8 Hz,^4J = 1 Hz, 1H, H3/H4/H5/H6/H10/H11/H12/H13), 7.28−7.33 (m, 1H, H3/H4/H5/H6/H10/H11/H12/H13), 7.04 (td,^3J = 8 Hz,^4J = 1 Hz, 1H, H18/H19), 6.42 (td,^3J = 8 Hz,^4J = 1 Hz, 1H, H18/H19), 6.32 (d,^2J = 14 Hz, 1H, H15), 5.98 (d,^2J = 16 Hz, 1H, H22), 5.32

https://doi.org/10.1021/acsorginorgau.2c00035
ACS Org. Inorg. Au 2022, 2, 511−524

(d,^3J = 8 Hz, 1H, H17/H20), 5.04 (d,^2J = 16 Hz, 1H, H22), 1.83 (s, 15H, Cp*). $^{13}C\{^1H\}$ NMR (100.61 MHz, $CDCl_3$): δ (ppm) = 166.8 (C, C28), 156.0 (CH, C27), 155.1 (C, C23), 140.8 (CH, C26), 134.4 (C, C16), 133.8 (C, C21), 132.3 (C, C2/C7/C9/C14), 131.7 (C, C2/C7/C9/C14), 131.3 (C, C2/C7/C9/C14), 131.2 (C, C2/C7/C9/C14), 130.1 (CH, C8), 130.0 (CH, C3/C4/C5/C6/C10/C11/C12/C13), 128.9 (CH, C3/C4/C5/C6/C10/C11/C12/C13), 127.8 (CH, C3/C4/C5/C6/C10/C11/C12/C13), 127.4 (CH, C3/C4/C5/C6/C10/C11/C12/C13), 126.7 (CH, C25), 126.5 (CH, C24), 125.8 (CH, C3/C4/C5/C6/C10/C11/C12/C13), 125.4 (CH, C3/C4/C5/C6/C10/C11/C12/C13), 124.8 (CH, C3/C4/C5/C6/C10/C11/C12/C13), 123.9 (CH, C18/C19), 123.8 (CH, C18/C19), 123.4 (C, C1), 122.6 (CH, C3/C4/C5/C6/C10/C11/C12/C13), 112.3 (CH, C17/C20), 110.8 (CH, C17/C20), 92.0 (C, Cp*),51.4 (NCH_2, C22), 47.9 (NCH_2, C15), 9.66 (CH_3, Cp*). MS (ESI$^+$) m/z: $[M - PF_6]^+$ calculated for $C_{38}H_{36}ClN_3Ir$ 762.2215; found 762.2218. Elemental analysis calculated for $C_{38}H_{36}ClN_3IrPF_6 \cdot 0.12\ H_2O \cdot 0.28\ C_6H_{14}$: C 51.05, H 4.34, N 4.50%; found: C 50.98, H 4.71, N 4.87%.

General Procedure for the Synthesis of Triazolyl-Functionalized NHC–$M^{II/III}$(cym/Cp*) Complexes (7a–7d)

A mixture of **5** and silver oxide in acetonitrile (20 mL) was refluxed in darkness for 1 day under nitrogen. A solution of $[M^{II/III}(cym/Cp^*)Cl_2]_2$ in acetonitrile (5 mL) was added to the reaction mixture that was refluxed for 4 days. NH_4PF_6 was added to the mixture, and the mixture was refluxed for another 24 h. The solvent was evaporated under reduced pressure, and then dichloromethane was added to the brown residue. The resultant suspension was filtered over Celite, and the filtrate was collected and evaporated under reduced pressure. The residue was dissolved in a minimal volume of dichloromethane (*ca.* 1 mL), and *n*-hexane was added to the solution, which led to the immediate formation of a brown precipitate. The precipitate was filtered, washed with *n*-hexane, and dried under a vacuum to afford the desired complexes.

Synthesis of {Chlorido[1-(anthracen-9-ylmethyl)-3-((1-benzyl-1,2,3-triazol-4-yl-*κN*)methyl)benzimidazol-2-ylidene-*κC*](*η*^{6}-*p*-cymene)ruthenium(II)} Hexafluorophosphate, 7a.

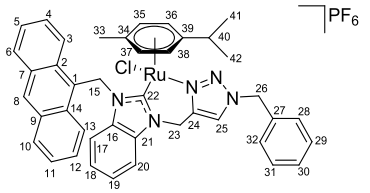

Compound **7a** was prepared by following the general procedure using **5** (100 mg, 0.16 mmol, 2.25 equiv), silver oxide (25 mg, 0.12 mmol, 1.50 equiv), $[Ru(cym)Cl_2]_2$ (49 mg, 0.08 mmol, 1.13 equiv), and NH_4PF_6 (81 mg, 0.45 mmol, 7.00 equiv). Yield: 77 mg (54%). ^1H NMR (400.13 MHz, $CDCl_3$): δ (ppm) = 8.65 (s, 1H, H8), 8.41 (d,^3J = 8 Hz, 1H, H3/H6/H10/H13), 8.20 (d,^3J = 8 Hz, 1H, H3/H6/H10/H13), 8.15 (d,^3J = 8 Hz, 1H, H3/H6/H10/H13), 8.06 (d,^3J = 8 Hz, 1H, H3/H6/H10/H13), 7.86 (s, 1H, H25), 7.49–7.59 (m, 3H, H4/H5/H11/H12), 7.46 (d,^3J = 8 Hz, 1H, H17/H20), 7.34–7.43 (m, 6H, H4/H5/H11/H12, H28, H29, H30, H31, H32), 7.19 (d,^2J = 16 Hz, 1H, H15), 7.03 (td,^3J = 8 Hz,^4J = 1 Hz, 1H, H18/H19), 6.64 (d,^2J = 16 Hz, 1H, H15), 6.52 (td,^3J = 8 Hz,^4J = 1 Hz, 1H, H18/H19), 5.96 (dd,^3J = 6 Hz, 1H, H35/H36/H37/H38), 5.78–5.34 (m, 2H, H35/H36/H37/H38), 5.59–5.73 (m, 4H, H17/H20, H26, H35/H36/H37/H38), 5.53 (dd,^3J = 6 Hz, 1H, H35/H36/H37/H38), 5.16 (d,^2J = 16 Hz, 1H, H23), 2.94 (sept,^3J = 7 Hz, 1H, H40), 2.23 (s, 3H, H33), 1.32 (d,^3J = 7 Hz, 3H, H41/H42), 1.22 (d,^3J = 7 Hz, 3H, H41/H42). $^{13}C\{^1H\}$ NMR (100.61 MHz, $CDCl_3$): δ (ppm) = 187.1 (C, C22), 141.4 (C, C24), 134.7 (C, C16/C21), 134.3 (C, C16/C21), 132.6 (C, C2/C7/C9/C14), 132.0 (C, C27), 131.4 (C, 2C, C2/C7/C9/C14), 131.2 (C, C2/C7/C9/C14), 130.1 (CH, C4/C5/C11/C12), 129.9 (CH, C8), 129.6 (CH, C30), 129.4 (CH, 2C, C29, C31), 129.1 (CH, C4/C5/C11/C12), 128.9 (CH, 2C, C28, C32), 127.5 (CH, 2C, C4/C5/C11/C12), 125.9 (CH, C3/C6/C10/C13), 125.3 (CH, C3/C6/C10/C13), 124.7 (CH, C3/C6/C10/C13), 124.1 (C, C1), 124.0 (CH, C25), 123.7 (CH, C18/C19), 123.6 (CH, C18/C19), 122.7 (CH, C3/C6/C10/C13), 112.9 (C, C34/C39), 111.9 (CH, C17/C20), 109.8 (CH, C17/C20), 101.4 (C, C34/C39), 88.4 (CH, C35/C36/C37/C38), 88.2 (CH, C35/C36/C37/C38), 87.8 (CH, C35/C36/C37/C38), 84.7 (CH, C35/C36/C37/C38), 56.1 (NCH_2, C26), 49.4 (NCH_2, C15), 40.7 (NCH_2, C23), 31.3 (CH, C40), 23.8 (CH_3, C41/C42), 20.7 (CH_3, C41/C42), 19.2 (CH_3, C33). MS (ESI$^+$) m/z: $[M - PF_6]^+$ calculated for $C_{42}H_{39}ClN_5Ru$ 750.1937; found 750.1928. Elemental analysis calculated for $C_{42}H_{39}ClN_5RuPF_6$: C 56.35, H 4.39, N 7.82%; found: C 56.69, H 4.76, N 7.71%.

Synthesis of {Chlorido[1-(anthracen-9-ylmethyl)-3-((1-benzyl-1,2,3-triazol-4-yl-*κN*)methyl)benzimidazol-2-ylidene-*κC*](*η*^{6}-*p*-cymene)osmium(II)} Hexafluorophosphate, 7b.

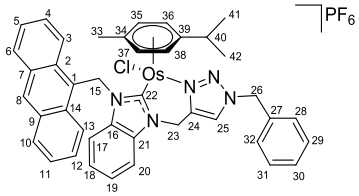

Compound **7b** was prepared by following the general procedure using **5** (100 mg, 0.16 mmol, 2.25 equiv), silver oxide (25 mg, 0.12 mmol, 1.50 equiv), $[Os(cym)Cl_2]_2$ (63 mg, 0.08 mmol, 1.13 equiv), and NH_4PF_6 (81 mg, 0.49 mmol, 7.00 equiv). Yield: 60 mg (38%). ^1H NMR (400.13 MHz, $CDCl_3$): δ (ppm) = 8.65 (s, 1H, H8), 8.44 (d,^3J = 8 Hz, 1H, H3/H6/H10/H13), 8.04–8.17 (m, 3H, H3/H4/H5/H6/H10/H11/H12/H13), 7.88 (s, 1H, H25), 7.48–7.56 (m, 3H, H3/H4/H5/H6/H10/H11/H12/H13), 7.43–7.47 (m, 2H, H3/H4/H5/H6/H10/H11/H12/H13, H17/H20), 7.35–7.43 (m, 5H, H28, H29, H30, H31, H32), 7.17 (d,^2J = 16 Hz, 1H, H15), 7.02 (td,^3J = 8 Hz,^4J = 1 Hz, 1H, H18/H19), 6.57 (d,^2J = 16 Hz, 1H, H15), 6.49 (td,^3J = 8 Hz,^4J = 1 Hz, 1H, H18/H19), 5.98 (d,^3J = 6 Hz, 1H, H35/H36/H37/H38), 5.87 (d,^3J = 6 Hz, 1H, H35/H36/H37/H38), 5.81 (d,^2J = 16 Hz, 1H, H23), 5.75 (d,^3J = 6 Hz, 1H, H35/H36/H37/H38), 5.72 (d,^2J = 16 Hz, 1H, H26), 5.67 (d,^3J = 6 Hz, 1H, H35/H36/H37/H38), 5.60–5.65 (m, 2H, H17/H20, H26), 5.14 (d,^2J = 16 Hz, 1H, H23), 2.88 (sept,^3J = 7 Hz, 1H, H40), 2.38 (s, 3H, H33), 1.27 (d,^3J = 7 Hz, 3H, H41/H42), 1.26 (d,^3J = 7 Hz, 3H, H41/H42). $^{13}C\{^1H\}$ NMR (100.61 MHz, $CDCl_3$): δ (ppm) = 170.9 (C, C22), 139.9 (C, C24), 134.3 (C, C16/C21), 133.6 (C, C16/C21), 132.6 (C, C27), 131.9 (C, C2/C7/C9/C14), 131.4 (C, C2/C7/C9/C14), 131.3 (C, C2/C7/C9/C14), 131.2 (C, C2/C7/C9/C14), 130.1 (CH, C3/C4/C5/C6/C10/C11/C12/C13), 129.9 (CH, C8), 129.4 (CH, 3C, C29, C30, C31), 129.1 (CH, C3/C4/C5/C6/C10/C11/C12/C13), 128.9 (CH, 2C, C28, 32), 127.5 (CH, C3/4/5/6/10/11/12/13), 127.4 (CH, C3/4/5/6/10/11/12/13), 125.8 (CH, C3/C4/C5/C6/C10/C11/C12/C13), 125.3 (CH, C3/C4/C5/C6/C10/C11/C12/C13), 124.5 (CH, C3/C4/C5/C6/C10/C11/C12/C13), 124.2 (C, C1), 123.7 (CH, 2C, C18, C19), 123.6 (CH, C25), 122.6 (CH, C3/C4/C5/C6/C10/C11/C12/C13), 112.1 (CH, C17/C20), 109.9 (CH, C17/C20), 103.9 (C, C34/C39), 93.4 (C, C34/C39), 79.9 (CH, C35/C36/C37/C38), 79.8 (CH, C35/C36/C37/C38), 79.1 (CH, C35/C36/C37/C38), 75.8 (CH, C35/C36/C37/C38), 55.9 (NCH_2, C26), 49.4 (NCH_2, C15), 40.9 (NCH_2, C23), 31.3 (CH, C40), 24.3 (CH_3, C41/C42), 20.7 (CH_3, C41/C42), 19.2 (CH_3, C33). MS (ESI$^+$) m/z: $[M - PF_6]^+$ calculated for $C_{42}H_{39}ClN_5Os$ 840.2495; found 840.2495. Elemental analysis calculated for $C_{42}H_{39}ClN_5OsPF_6$: C 51.24, H 3.99, N 7.11%; found: C 51.29, H 4.10, N 7.43%.

Synthesis of {Chlorido[1-(anthracen-9-ylmethyl)-3-((1-benzyl-1,2,3-triazol-4-yl-*κN*)methyl)benzimidazol-2-ylidene-*κC*]-

https://doi.org/10.1021/acsorginorgau.2c00035
ACS Org. Inorg. Au 2022, 2, 511–524

(η^5-pentamethylcyclopentadienyl)rhodium(III)} Hexafluorophosphate, 7c.

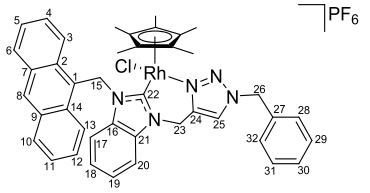

Compound **7c** was prepared by following the general procedure using **5** (100 mg, 0.16 mmol, 2.25 equiv), silver oxide (25 mg, 0.12 mmol, 1.50 equiv), $[Rh(Cp^*)Cl_2]_2$ (49 mg, 0.08 mmol, 1.13 equiv), and NH_4PF_6 (81 mg, 0.45 mmol, 7.00 equiv). Yield: 57 mg (36%). ^{1}H NMR (400.13 MHz, $CDCl_3$): δ (ppm) = 8.65 (s, 1H, H8), 8.41 (d,^3J = 8 Hz, 1H, H3/H6/H10/H13), 8.15−8.20 (m, 3H, H3/H4/H5/H6/H10/H11/H12/H13, H25), 8.02 (d,^3J = 8 Hz, 1H, H3/H6/H10/H13), 7.55−7.61 (m, 3H, H3/H4/H5/H6/H10/H11/H12/H13, H17/20), 7.51 (d,^2J = 16 Hz, 1H, H15), 7.37−7.46 (m, 6H, H3/H4/H5/H6/H10/H11/H12/H13, H28, H29, H30, H31, H32), 7.31−7.36 (m, 1H, H3/H4/H5/H6/H10/H11/H12/H13), 7.05 (td,^3J = 8 Hz,^4J = 1 Hz, 1H, H18/H19), 6.46 (td,^3J = 8 Hz,^4J = 1 Hz, 1H, H18/H19), 6.34 (d,^2J = 16 Hz, 1H, H15), 5.99 (d,^2J = 16 Hz, 1H, H23), 5.69 (s, 2H, H26), 5.35 (d,^3J = 8 Hz, 1H, H17/H20), 5.15 (d,^2J = 16 Hz, 1H, H23), 1.81 (s, 15H, Cp*).

^{13}C{^{1}H} NMR (100.61 MHz, $CDCl_3$): δ (ppm) = 180.7 (d,^1J = 51 Hz, C , C22), 141.3 (C, C24), 134.5 (C, C16/C21), 134.4 (C, C16/C21), 132.8 (C, C2/C7/C9/C14), 132.5 (C, C2/C7/C9/C14), 131.7 (C, C27), 131.4 (C, C2/C7/C9/C14), 131.2 (C, C2/C7/C9/C14), 130.1 (CH, 2C, C3/C4/C5/C6/C8/C10/C11/C12/C13), 129.5 (CH, C30), 129.4 (CH, 2C, C29, C31), 128.9 (CH, 2C, C28, C32), 128.8 (CH, C3/C4/C5/C6/C10/C11/C12/C13), 127.6 (CH, 2C, C3/C4/C5/C6/C10/C11/C12/C13), 125.9 (CH, C3/C4/C5/C6/C10/C11/C12/C13), 125.2 (CH, C25), 125.1 (CH, 2C, C3/C4/C5/C6/C10/C11/C12/C13), 124.0 (CH, C18/C19), 123.9 (CH, C18/C19), 123.5 (C, C1), 112.5 (CH, C3/C4/C5/C6/C10/C11/C12/C13), 112.3 (CH, C17/C20), 110.5 (CH, C17/C20), 99.4 (d,^1J = 7 Hz, C, Cp*), 56.2 (NCH_2, C26), 48.7 (NCH_2, C15), 40.7 (NCH_2, C23), 9.9 (CH_3, Cp*). MS (ESI$^+$) *m/z*: $[M - PF_6]^+$ calculated for $C_{42}H_{40}ClN_5Rh$ 752.2027; found 752.2023. Elemental analysis calculated for $C_{42}H_{40}ClN_5RhPF_6 \cdot 0.05\ H_2O$: C 56.11, H 4.50, N 7.79%; found: C 56.48, H 4.88, N 7.57%.

Synthesis of {Chlorido[1-(anthracen-9-ylmethyl)-3-((1-benzyl-1,2,3-triazol-4-yl-*κN*)methyl)benzimidazol-2-ylidene-*κC*]-(η^5-pentamethylcyclopentadienyl)iridium(III)} Hexafluorophosphate, 7d.

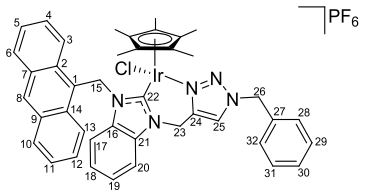

Compound **7d** was prepared by following the general procedure using **5** (86 mg, 0.14 mmol, 2.25 equiv), silver oxide (19 mg, 0.08 mmol, 1.38 equiv), $[Ir(Cp^*)Cl_2]_2$ (49 mg, 0.06 mmol, 1.00 equiv), and NH_4PF_6 (67 mg, 0.41 mmol, 6.75 equiv). Yield: 35 mg (29%). ^{1}H NMR (400.13 MHz, $CDCl_3$): δ (ppm) = 8.66 (s, 1H, H8), 8.43 (d,^3J = 8 Hz, 1H, H3/H4/H5/H6/H10/H11/H12/H13), 8.20 (s, 1H, H25), 8.14−8.18 (m, 2H, H3/H4/H5/H6/H10/H11/H12/H13), 8.03 (d,^3J = 8 Hz, 1H, H3/H4/H5/H6/H10/H11/H12/H13), 7.49−7.61 (m, 3H, H3/H4/H5/H6/H10/H11/H12/H13, H17/H20), 7.38−7.46 (m, 7H, H3/H4/H5/H6/H10/H11/H12/H13, H15, H28, H29, H30, H31, H32), 7.32−7.37 (m, 1H, H3/H4/H5/H6/H10/H11/H12/H13), 7.02 (t,^3J = 8 Hz, 1H, H18/H19), 6.43 (t,^3J = 8 Hz, 1H, H18/H19), 6.29 (d,^2J = 15 Hz, 1H, H15), 5.96 (d,^2J = 16 Hz, 1H, H23), 5.70 (s, 2H, H26), 5.32 (d,^3J = 8 Hz, 1H, H17/H20), 5.04 (d,^2J = 16 Hz, 1H, H23), 1.83 (s, 15H, Cp*). ^{13}C{^{1}H} NMR (100.61 MHz, $CDCl_3$): δ (ppm) = 164.7 (C, C22), 140.6 (C, C24), 134.2 (C, C16/C21), 133.9 (C, C16/C21), 132.8 (C, C2/C7/C9/C14), 132.5 (C, C2/C7/C9/C14), 131.7 (C, C27), 131.3 (C, C2/C7/C9/C14), 131.2 (C, C2/C7/C9/C14), 130.2 (CH, C8), 130.1 (CH, C3/C4/C5/C6/C10/C11/C12/C13), 129.5 (CH, C30), 129.4 (CH, 2C, C29, C31), 128.9 (CH, 2C, C28, C32), 128.8 (CH, C3/C4/C5/C6/C10/C11/C12/C13), 127.6 (CH, C3/C4/C5/C6/C10/C11/C12/C13), 127.5 (CH, C3/C4/C5/C6/C10/C11/C12/C13), 125.9 (CH, C3/C4/C5/C6/C10/C11/C12/C13), 125.2 (CH, C3/C4/C5/C6/C10/C11/C12/C13), 124.9 (CH, C25), 124.8 (CH, C3/C4/C5/C6/C10/C11/C12/C13), 124.0 (CH, C18/C19), 123.9 (CH, C18/C19), 123.5 (C, C1), 122.5 (CH, C3/C4/C5/C6/C10/C11/C12/C13), 112.3 (CH, C17/C20), 110.5 (CH, C17/C20), 92.2 (C, Cp*),56.2 (NCH_2, C26), 48.5 (NCH_2, C15), 40.9 (NCH_2, C23), 9.64 (CH_3, Cp*). MS (ESI$^+$) *m/z*: $[M - PF_6]^+$ calculated for $C_{42}H_{40}ClN_5Ir$ 842.2601; found 842.2599. Elemental analysis calculated for $C_{42}H_{40}ClN_5IrPF_6$: C 51.09, H 4.08, N 7.09%; found: C 51.42, H 4.41, N 6.90%.

Synthesis of {[1-((1-Benzyl-1,2,3-triazol-4-yl-*κN*)methyl)3-({10-[(η^5−2,3,4,5-tetramethylcyclopentadienyl)methyl]-9,10-dihydroanthracene-9-yl-κ^2C}methyl)benzimidazol-2-ylidene-*κC*]rhodium(III)} Triflate, 8′.

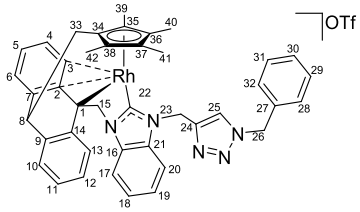

A mixture of **5** (100 mg, 0.16 mmol, 2 equiv) and silver oxide (37 mg, 0.16 mmol, 2 equiv) in acetonitrile (20 mL) was refluxed in darkness for 1 day under nitrogen. A solution of $[Rh(Cp^*)Cl_2]_2$ (49 mg, 0.08 mmol, 1 equiv) in acetonitrile (5 mL) was added to the reaction mixture that was then refluxed for 4 days. AgOTf (41 mg, 0.16 mmol, 2 equiv) was added to the mixture that was refluxed for another 48 h. The solvent was evaporated under reduced pressure, and then dichloromethane was added to the residue. The resultant suspension was filtered over Celite, and the filtrate was collected and evaporated under reduced pressure. The residue was dissolved in a minimal volume of dichloromethane (*ca.* 1 mL), and *n*-hexane was added to the solution, which led to the immediate formation of a blue precipitate. The precipitate was filtered, washed with *n*-hexane, and dried under vacuum to afford the desired complexes. Yield: 49 mg (38%). ^{1}H NMR (400.13 MHz, $CDCl_3$): δ (ppm) = 7.94 (s, 1H, H25), 7.63 (t,^3J = 8 Hz, 2H, H4/H5/H11/H12), 7.43 (d,^3J = 8 Hz, 1H, H3/H6/H10/H13), 7.35−7.39 (m, 4H, H3/H6/H10/H13, H18, H19), 7.28−7.34 (m, 6H, H3/H6/H10/H13, H28, H29, H30, H31, H32), 7.21 (t,^3J = 8 Hz, 2H, H4/H5/H11/H12), 6.52 (d,^3J = 8 Hz, 2H, H17/H20), 5.94 (s, 2H, H23), 5.51 (s, 2H, H26), 4.81 (t,^3J = 4 Hz, 1H, H8), 4.58 (s, 2H, H15), 2.22 (d,^3J = 4 Hz, 2H, H33), 1.77 (s, 6H, H39/H40/H41/H42), 0.40 (s, 6H, H39/H40/H41/H42). ^{13}C{^{1}H} NMR (100.61 MHz, $CDCl_3$): δ (ppm) = 129.8 (CH, 3C, C3/C4/C5/C6/C10/C11/C12/C13), 128.9 (CH, 2C, C4/C5/C11/C12, C28/C29/C30/C31/C32), 128.7 (CH, 2C, C28/C29/C30/C31/C32), 128.5 (CH, C28/C29/C30/C31/C32), 128.4 (CH, C28/C29/C30/C31/C32), 127.9 (CH, 2C, C4/C5/C11/C12), 124.4 (CH, C3/C6/C10/C13), 124.2 (CH, C3/C6/C10/C13), 123.7 (CH, C25), 118.3 (CH, C17, C20), 112.1 (CH, C18/C19), 110.9 (CH, C18/C19), 54.2 (NCH_2, C26), 50.4 (NCH_2, C15), 45.3 (CH, C8), 44.6 (NCH_2, C23), 29.4 (CH_2, C33), 11.0 (CH_3, C39/C40/C41/C42), 5.89 (CH_3, C39/C40/C41/C42). MS (ESI$^+$) *m/z*: $[M - OTf]^+$ calculated for $C_{42}H_{39}N_5Rh$ 716.2255; found 716.2266. Elemental analysis calculated for $C_{43}H_{39}N_5RhF_3O_3S \cdot 1.3\ H_2O$: C 58.08, H 4.72, N 7.88%; found: C 57.76, H 4.78, N 7.71%.

■ ASSOCIATED CONTENT

Supporting Information

The Supporting Information is available free of charge at https://pubs.acs.org/doi/10.1021/acsorginorgau.2c00035.

https://doi.org/10.1021/acsorginorgau.2c00035
ACS Org. Inorg. Au 2022, 2, 511−524

ESI-MS characterization data, reactivity studies by MS and NMR spectroscopy, density functional theory calculations (procedure, benchmarking, and additional figures), UV−vis spectra, fluorescence spectra, X-ray crystallography data and data collection parameters and ^{1}H, $^{13}C\{^{1}H\}$ DEPTQ and 2D NMR and ESI-mass spectra used in the characterization of compounds (PDF)

Accession Codes

CCDC 2101573−2101574 contain the supplementary crystallographic data for this paper. These data can be obtained free of charge via www.ccdc.cam.ac.uk/data_request/cif, or by emailing data_request@ccdc.cam.ac.uk, or by contacting The Cambridge Crystallographic Data Centre, 12 Union Road, Cambridge CB2 1EZ, UK; fax: +44 1223 336033.

AUTHOR INFORMATION

Corresponding Authors

Andrew D. Phillips − *School of Chemistry, University College Dublin, Dublin 4 D04 V1W8, Ireland;* orcid.org/0000-0001-5599-6499; Email: andrew.phillips@ucd.ie

Christian G. Hartinger − *School of Chemical Sciences, The University of Auckland, Auckland 1142, New Zealand;* orcid.org/0000-0001-9806-0893; Email: c.hartinger@auckland.ac.nz

Authors

Betty Y.T. Lee − *School of Chemical Sciences, The University of Auckland, Auckland 1142, New Zealand;* orcid.org/0000-0001-5190-2993

Muhammad Hanif − *School of Chemical Sciences, The University of Auckland, Auckland 1142, New Zealand;* orcid.org/0000-0002-2256-2317

Tilo Söhnel − *School of Chemical Sciences, The University of Auckland, Auckland 1142, New Zealand;* orcid.org/0000-0003-4472-5807

Complete contact information is available at: https://pubs.acs.org/10.1021/acsorginorgau.2c00035

Notes

The authors declare no competing financial interest.

ACKNOWLEDGMENTS

We thank the University of Auckland for its financial support. B.Y.T.L. thanks the University of Auckland for a University of Auckland Doctoral Scholarship. M.H. is supported by a Sir Charles Hercus Health Research Fellowship through the Health Research Council of New Zealand. We are grateful to Tanya Groutso for collecting the single-crystal X-ray diffraction data and to Mansa Nair for the ESI-MS data. A.D.P. thanks Science Foundation Ireland (SFI) for a Stokes Lectureship held at the School of Chemistry, UCD. The authors are grateful for access to computing facilities (Kay cluster) owned and operated by the Irish Centre for High-End Computing (ICHEC).

REFERENCES

(1) Lam, N. Y. S.; Truong, D.; Burmeister, H.; Babak, M. V.; Holtkamp, H. U.; Movassaghi, S.; Ayine-Tora, D. M.; Zafar, A.; Kubanik, M.; Oehninger, L.; Söhnel, T.; Reynisson, J.; Jamieson, S. M. F.; Gaiddon, C.; Ott, I.; Hartinger, C. G. From Catalysis to Cancer: Toward Structure−Activity Relationships for Benzimidazol-2-ylidene-Derived N-Heterocyclic-Carbene Complexes as Anticancer Agents. *Inorg. Chem.* **2018**, *57*, 14427−14434.

(2) Bellemin-Laponnaz, S. N-Heterocyclic Carbene Platinum Complexes: A Big Step Forward for Effective Antitumor Compounds. *Eur. J. Inorg. Chem.* **2020**, *2020*, 10−20.

(3) Curran, D.; Müller-Bunz, H.; Bär, S. I.; Schobert, R.; Zhu, X.; Tacke, M. Novel Anticancer NHC*-Gold(I) Complexes Inspired by Lepidiline A. *Molecules* **2020**, *25*, 3474.

(4) Fabbrini, M. G.; Cirri, D.; Pratesi, A.; Ciofi, L.; Marzo, T.; Guerri, A.; Nistri, S.; Dell'Accio, A.; Gamberi, T.; Severi, M.; Bencini, A.; Messori, L. A Fluorescent Silver(I) Carbene Complex with Anticancer Properties: Synthesis, Characterization, and Biological Studies. *ChemMedChem* **2019**, *14*, 182−188.

(5) Teyssot, M.-L.; Jarrousse, A.-S.; Chevry, A.; De Haze, A.; Beaudoin, C.; Manin, M.; Nolan, S. P.; Díez-González, S.; Morel, L.; Gautier, A. Toxicity of Copper(I)−NHC Complexes Against Human Tumor Cells: Induction of Cell Cycle Arrest, Apoptosis, and DNA Cleavage. *Chem. − Eur. J.* **2009**, *15*, 314−318.

(6) Wang, C.; Liu, J.; Tian, Z.; Tian, M.; Tian, L.; Zhao, W.; Liu, Z. Half-sandwich iridium N-heterocyclic carbene anticancer complexes. *Dalton Trans.* **2017**, *46*, 6870−6883.

(7) Daubit, I. M.; Sullivan, M. P.; John, M.; Goldstone, D. C.; Hartinger, C. G.; Metzler-Nolte, N. A Combined Spectroscopic and Protein Crystallography Study Reveals Protein Interactions of Rh^{I}(NHC) Complexes at the Molecular Level. *Inorg. Chem.* **2020**, *59*, 17191−17199.

(8) Movassaghi, S.; Singh, S.; Mansur, A.; Tong, K. K. H.; Hanif, M.; Holtkamp, H. U.; Söhnel, T.; Jamieson, S. M. F.; Hartinger, C. G. (Pyridin-2-yl)-NHC Organoruthenium Complexes: Antiproliferative Properties and Reactivity toward Biomolecules. *Organometallics* **2018**, *37*, 1575−1584.

(9) Jantke, D.; Cokoja, M.; Pöthig, A.; Herrmann, W. A.; Kühn, F. E. Synthesis and Characterization of Highly Water Soluble Ruthenium(II) and Osmium(II) Complexes Bearing Chelating Sulfonated N-Heterocyclic Carbene Ligands. *Organometallics* **2013**, *32*, 741−744.

(10) Ndagi, U.; Mhlongo, N.; Soliman, M. E. Metal complexes in cancer therapy - an update from drug design perspective. *Drug Des., Dev. Ther.* **2017**, *Volume11*, 599−616.

(11) Oehninger, L.; Rubbiani, R.; Ott, I. N-Heterocyclic carbene metal complexes in medicinal chemistry. *Dalton Trans.* **2013**, *42*, 3269−3284.

(12) Truong, D.; Sullivan, M. P.; Tong, K. K. H.; Steel, T. R.; Prause, A.; Lovett, J. H.; Andersen, J. W.; Jamieson, S. M. F.; Harris, H. H.; Ott, I.; Weekley, C. M.; Hummitzsch, K.; Söhnel, T.; Hanif, M.; Metzler-Nolte, N.; Goldstone, D. C.; Hartinger, C. G. Potent Inhibition of Thioredoxin Reductase by the Rh Derivatives of Anticancer M(arene/Cp*)(NHC)Cl_2 Complexes. *Inorg. Chem.* **2020**, *59*, 3281−3289.

(13) Prast-Nielsen, S.; Cebula, M.; Pader, I.; Arnér, E. S. J. Noble metal targeting of thioredoxin reductase - covalent complexes with thioredoxin and thioredoxin-related protein of 14kDa triggered by cisplatin. *Free Radical Biol. Med.* **2010**, *49*, 1765−1778.

(14) Gandin, V.; Fernandes, A. Metal- and Semimetal-Containing Inhibitors of Thioredoxin Reductase as Anticancer Agents. *Molecules* **2015**, *20*, 12732−12756.

(15) Zhang, J.; Li, X.; Han, X.; Liu, R.; Fang, J. Targeting the Thioredoxin System for Cancer Therapy. *Trends Pharmacol. Sci.* **2017**, *38*, 794−808.

(16) Weiss, A.; Berndsen, R. H.; Dubois, M.; Müller, C.; Schibli, R.; Griffioen, A. W.; Dyson, P. J.; Nowak-Sliwinska, P. In vivo anti-tumor activity of the organometallic ruthenium(II)-arene complex [Ru(η^6-*p*-cymene)Cl_2(pta)] (RAPTA-C) in human ovarian and colorectal carcinomas. *Chem. Sci.* **2014**, *5*, 4742−4748.

(17) Aird, R. E.; Cummings, J.; Ritchie, A. A.; Muir, M.; Morris, R. E.; Chen, H.; Sadler, P. J.; Jodrell, D. I. *In vitro* and in vivo activity and cross resistance profiles of novel ruthenium (II) organometallic arene complexes in human ovarian cancer. *Br. J. Cancer* **2002**, *86*, 1652−1657.

(18) Dabiri, Y.; Schmid, A.; Theobald, J.; Blagojevic, B.; Streciwilk, W.; Ott, I.; Wölfl, S.; Cheng, X. A Ruthenium(II) *N*-Heterocyclic Carbene (NHC) Complex with Naphthalimide Ligand Triggers Apoptosis in Colorectal Cancer Cells via Activating the ROS-p38 MAPK Pathway. *Int. J. Mol. Sci.* **2018**, *19*, 3964.
(19) Hanif, M.; Arshad, J.; Astin, J. W.; Rana, Z.; Zafar, A.; Movassaghi, S.; Leung, E.; Patel, K.; Söhnel, T.; Reynisson, J.; Sarojini, V.; Rosengren, R. J.; Jamieson, S. M. F.; Hartinger, C. G. A Multitargeted Approach: Organorhodium Anticancer Agent Based on Vorinostat as a Potent Histone Deacetylase Inhibitor. *Angew. Chem., Int. Ed. Engl.* **2020**, *59*, 14609−14614.
(20) Tremlett, W. D. J.; Goodman, D. M.; Steel, T. R.; Kumar, S.; Wieczorek-Błauż, A.; Walsh, F. P.; Sullivan, M. P.; Hanif, M.; Hartinger, C. G. Design concepts of half-sandwich organoruthenium anticancer agents based on bidentate bioactive ligands. *Coord. Chem. Rev.* **2021**, *445*, No. 213950.
(21) Steel, T. R.; Walsh, F.; Wieczorek-Błauż, A.; Hanif, M.; Hartinger, C. G. Monodentately-coordinated bioactive moieties in multimodal half-sandwich organoruthenium anticancer agents. *Coord. Chem. Rev.* **2021**, *439*, No. 213890.
(22) Adhireksan, Z.; Davey, G. E.; Campomanes, P.; Groessl, M.; Clavel, C. M.; Yu, H.; Nazarov, A. A.; Yeo, C. H. F.; Ang, W. H.; Dröge, P.; Rothlisberger, U.; Dyson, P. J.; Davey, C. A. Ligand substitutions between ruthenium−cymene compounds can control protein versus DNA targeting and anticancer activity. *Nat. Commun.* **2014**, *5*, 3462.
(23) Nabiyeva, T.; Marschner, C.; Blom, B. Synthesis, structure and anti-cancer activity of osmium complexes bearing π-bound arene substituents and phosphane Co-Ligands: A review. *Eur. J. Med. Chem.* **2020**, *201*, No. 112483.
(24) Oehninger, L.; Spreckelmeyer, S.; Holenya, P.; Meier, S. M.; Can, S.; Alborzinia, H.; Schur, J.; Keppler, B. K.; Wölfl, S.; Ott, I. Rhodium(I) *N*-Heterocyclic Carbene Bioorganometallics as in Vitro Antiproliferative Agents with Distinct Effects on Cellular Signaling. *J. Med. Chem.* **2015**, *58*, 9591−9600.
(25) Bolaño, S.; Albinati, A.; Bravo, J.; Caporali, M.; Gonsalvi, L.; Male, L.; Mar Rodríguez-Rocha, M.; Rossin, A.; Peruzzini, M. Synthesis and reactivity of rhodium(III) pentamethylcyclopentadienyl complexes of *N*−*B*−PTA(BH_3): X-ray crystal structures of [Cp*$RhCl_2${*N*−*B*}−PTA(BH_3)] and [Cp*Rh{*N*−*B*−PTA(BH_3)}-(η^2-CH_2=CHPh)]. *J. Organomet. Chem.* **2008**, *693*, 2397−2406.
(26) Liu, Z.; Sadler, P. J. Organoiridium Complexes: Anticancer Agents and Catalysts. *Acc. Chem. Res.* **2014**, *47*, 1174−1185.
(27) Lee, B. Y. T.; Sullivan, M. P.; Yano, E.; Tong, K. K. H.; Hanif, M.; Kawakubo-Yasukochi, T.; Jamieson, S. M. F.; Soehnel, T.; Goldstone, D. C.; Hartinger, C. G. Anthracenyl Functionalization of Half-Sandwich Carbene Complexes: In Vitro Anticancer Activity and Reactions with Biomolecules. *Inorg. Chem.* **2021**, *60*, 14636−14644.
(28) Lee, B. Y. T.; Phillips, A. D.; Hanif, M.; Tong, K. K. H.; Söhnel, T.; Hartinger, C. G. Heptadentate, octadentate or even nonadentate? Denticity in the unexpected formation of an all-carbon donor atom ligand in Rh^{III}(Cp*)(anthracenyl-NHC) complexes. *Inorg. Chem.* **2021**, *60*, 8734−8741.
(29) Segarra, C.; Mas-Marzá, E.; Benítez, M.; Mata, J. A.; Peris, E. Unconventional Reactivity of Imidazolylidene Pyridylidene Ligands in Iridium(III) and Rhodium(III) Complexes. *Angew. Chem., Int. Ed. Engl.* **2012**, *51*, 10841−10845.
(30) Banerjee, S.; Soldevila-Barreda, J. J.; Wolny, J. A.; Wootton, C. A.; Habtemariam, A.; Romero-Canelón, I.; Chen, F.; Clarkson, G. J.; Prokes, I.; Song, L.; O'Connor, P. B.; Schünemann, V.; Sadler, P. J. New activation mechanism for half-sandwich organometallic anticancer complexes. *Chem. Sci.* **2018**, *9*, 3177−3185.
(31) Thomas, H. P.; Marr, A. C.; Morgan, P. J.; Saunders, G. C. Tethering of Pentamethylcyclopentadienyl and N-Heterocycle Stabilized Carbene Ligands by Intramolecular 1,4-Addition to a Polyfluorophenyl Substituent. *Organometallics* **2018**, *37*, 1339−1341.
(32) Tong, K. K. H.; Hanif, M.; Lovett, J. H.; Hummitzsch, K.; Harris, H. H.; Söhnel, T.; Jamieson, S. M. F.; Hartinger, C. G. Thiourea-Derived Chelating Ligands and Their Organometallic Compounds: Investigations into Their Anticancer Activity. *Molecules* **2020**, *25*, 3661.
(33) Gerlach, D. L.; Siek, S.; Burks, D. B.; Tesh, J. M.; Thompson, C. R.; Vasquez, R. M.; White, N. J.; Zeller, M.; Grotjahn, D. B.; Papish, E. T. Ruthenium(II) and iridium(III) complexes of *N*-heterocyclic carbene and pyridinol derived bidentate chelates: Synthesis, characterization, and reactivity. *Inorg. Chim. Acta* **2017**, *466*, 442−450.
(34) O'Connor, C.; Lawlor, D. C.; Robinson, C.; Müller-Bunz, H.; Phillips, A. D. Comprehensive Experimental and Computational Study of η6-Arene Ruthenium(II) and Osmium(II) Complexes Supported by Sulfur Analogues of the β-Diketiminate Ligand. *Organometallics* **2018**, *37*, 1860−1875.
(35) Biedermann, G.; Sillén, L. G. Studies on the Hydrolysis of Metal Ions. Part 30. A Critical Survey of the Solubility Equilibria of Ag_2O. *Acta Chem. Scand.* **1960**, *14*, 717−725.
(36) Hoard, D. W.; Sharp, P. R. Chemistry of [Cp*Rh(μ-Cl)]$_2$ and its dioxygen and nitrosobenzene insertion products. *Inorg. Chem.* **1993**, *32*, 612−620.
(37) Kang, J. W.; Moseley, K.; Maitlis, P. M. Pentamethylcyclopentadienylrhodium and -iridium halides. I. Synthesis and properties. *J. Am. Chem. Soc.* **1969**, *91*, 5970−5977.
(38) White, C.; Yates, A.; Maitlis, P. M.; Heinekey, D. M., (η^5-Pentamethylcyclopentadienyl)Rhodium and -Iridium Compounds. In *Inorg. Synth.*, John Wiley & Sons, Inc.: 2007; pp. 228−234.
(39) Sheldrick, G. M. A short history of SHELX. *Acta Crystallogr., Sect. A: Found. Crystallogr.* **2008**, *A64*, 112−122.
(40) Dolomanov, O. V.; Bourhis, L. J.; Gildea, R. J.; Howard, J. A. K.; Puschmann, H. OLEX2: a complete structure solution, refinement and analysis program. *J. Appl. Crystallogr.* **2009**, *42*, 339−341.
(41) Sheldrick, G. Crystal structure refinement with SHELXL. *Acta Crystallogr., Sect. C: Cryst. Struct. Commun.* **2015**, *71*, 3−8.

https://doi.org/10.1021/acsorginorgau.2c00035
ACS Org. Inorg. Au 2022, 2, 511−524